MASTER THESIS IN MEDICAL CELL BIOLOGY

INSIGHTS INTO THE CELLULAR ROLE OF SERINE19 PHOSPHORYLATION IN TYROSINE HYDROXYLASE

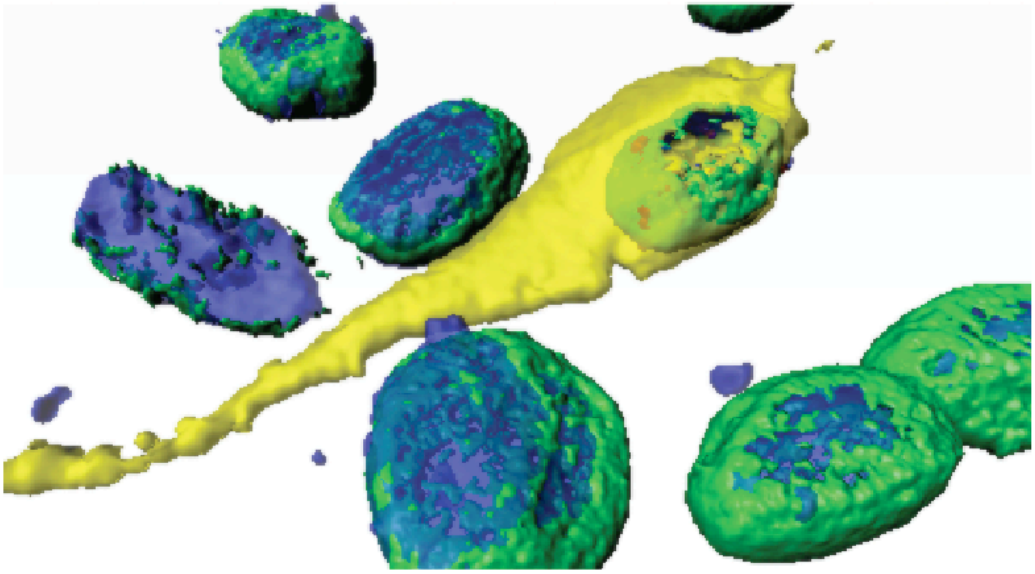

KUNWAR JUNG KC

This thesis is submitted in partial fulfilment of the requirements for the degree of Master of Science

THE DEPARTMENT OF BIOMEDICINE
FACULTY OF MEDICINE AND DENTISTRY
UNIVERSITY OF BERGEN
JUNE 2016

Acknowledgements

First, I would like to thank my supervisor Professor Aurora Martinez for giving me the opportunity to do research in her group. Prof. Martinez's guidance and encouragement have been a constant source of motivation for the delivery of this piece of work. After more than a year of being part of your research group, I am still day after day amazed by your ability to transfer energy to people in such an effective manner.

I would like to express my deepest gratitude to my co-supervisor Dr. Ana Jorge-Finnigan. Your guidance, insight, knowledge and support were invaluable throughout the Master's thesis. Your passion, enthusiasm and sharp minds for science showed me what a real scientist is. I feel lucky to be one of your students and what I have learned from you will be the treasure of my life.

"No man is an island". I feel lucky to be a part of the Biorecognition research group and I am happy to meet so many great people during my academic year. Thank you all for your input, encouragement and lunch break talks, I appreciate it a lot. Ming, thank you for help in the lab. Anne, thank you for inviting me to fishing trip, it was so much fun. Marte, thank you for your support and encouragement. I would like to thank all PhD students Helene, Maite and Oscar for being friendly, supportive and encouraging. Helene and Maite thank you for letting me refer to you thesis report, it was a great help. I would like to thank other Masters students, Pradosh, Ellen and Fredrick for being in the same boat as me and sharing all the frustration, it was encouraging to see you all work hard.

I would like to thank my Norwegian foster family, The Møll family, Jon, Irene, Rolf and Tore specially, thank you for inviting me to all the dinner parties and jamming session. You guys made my days easier in Norway and made me feel like home.

Finally, my family deserves special recognition, specially my parents Ram Bahadur KC and Sabitri KC. Your unconditional love and support have been my driving force of going forward. I feel blessed with all your love, encouragement and faith in me.

ABSTRACT

Tyrosine hydroxylase (TH) is the rate limiting enzyme that catalyzes the first step in the biosynthesis of catecholamines. The posttranslational modification of its regulatory domain controls the regulation of TH enzyme activity. Different kinases are responsible for the phosphorylation of the enzyme at Thr8, Ser19, Ser31 and Ser40 N terminal residues. It is well established that phosphorylation at Ser31 and Ser40 (THpSer31 and THpSer40, respectively) leads to an increase of TH activity. However, phosphorylation of Ser19 does not directly increase TH activity but induces its binding to the 14-3-3 protein, leading to the enhancement of TH activity through a mechanism yet not fully understood. The main goal of this work was to investigate the cellular role of Ser19 phosphorylation in TH. Site-directed mutagenesis was used to substitute Ser residue with Ala and Glu at position 19 of recombinant V5-tagged TH to create a phospho-null (V5-TH-S19A) and phospho-mimic mutant (V5-TH-S19E), respectively. Native-PAGE analysis showed that there is no significant difference in the oligomeric state of TH in nuclear and cytosolic fractions of neuroblastoma cells, regardless of the phosphorylation state of Ser19. Immunofluorescence (IF) analysis of the subcellular distribution of endogenous THpSer19 showed that it was predominantly distributed in the nucleus of neuroblastoma cells. However, Western blot results showed that the band intensity for THpSer19 in the cytosolic fraction was stronger than the band found in the nuclear fraction. Proximity ligation assay (PLA) suggested that the amount of TH present in the nucleus is phosphorylated at Ser19. Western blot and immunofluorescence analysis showed that the phospho-site mutants did not accumulate preferentially in the nucleus or in the cytosol. Both IF and PLA analysis showed that 14-3-3 proteins are distributed in the cytoplasm and nucleus of neuroblastoma cells. PLA analysis indicated that also in the nucleus THpSer19 interacts with 14-3-3 protein. These results, thus, have an impact on fundamental understanding of the distribution of THpSer19 and one of the binding partners in nucleus, such as 14-3-3γ.

ABBREVIATIONS

AA	amino acid
AAAH	aromatic amino acid hydroxylase
AU	arbitrary unit
BH4	tetrahydrobiopterin
BN-PAGE	blue native polyacrylamide gel electrophoresis
CaMPK	calcium-calmodulin-dependent protein kinase
CMV	cytomegalovirus
CN-PAGE	clear native polyacrylamide gel electrophoresis
ERK	extracellular regulated kinases
ES	enzyme-substrate complex
GFP	green fluorescent protein
HNF	hepatocyte nuclear factor
IF	immunofluorescence
L-DOPA	L-3,4-dihydroxyphenylalanine
LZ	leucine zipper
MAPKAPK	mitogen-activated-protein kinase-activating protein kinase
PCD	pterin-4a-carbinolamine dehydratase
PCR	polymerase chain reaction
PK	protein kinase
PKA	protein kinase A
PLA	proximity ligation assay
PP	protein phosphatase
PRAK	p38 regulated/activated kinase
PTM	post translational modification
PAH	phenylalanine hydroxylase
PVDF	polyvinylidene fluoride
RCA	rolling circle amplification
TH	tyrosine hydroxylase
TPH	tryptophan hydroxylase
SD	standard deviation
SDM	site-directed mutagenesis
SDS-PAGE	sodium dodecylsulfate polyacrylamide gel electrophoresis
Wt	wildtype

Abbreviations of chemicals can be found in the chemical list (section 3.5).

Table of Contents

1. INTRODUCTION

1.1 Enzyme

Enzymes are macromolecular biological catalysts of life. The biochemical reactions that occur up to the rate at which biological processes takes place in living organisms are regulated by enzymes. The first enzyme to be discovered was “diastase”, now known as “amylase”, by Payen & Persoz in 1833 [1]. In 1926, Sumner demonstrated that enzymes are actually proteins [2], as a result, he was awarded the Nobel Prize in Chemistry in 1946. During the 1960s, Anfinsen’s study shed light on the dynamic nature of protein structure and contributed in the development of proteolytic methods [3, 4]. Subsequent research on the active site and catalytic mechanism of enzymes by Cornforth and co-workers introduced mechanistic enzymology as a new scientific discipline.

Enzymes are linear chains of amino acids that fold to create a tridimensional structure. Although the catalytic activity of the enzyme can be determined by the amino acids sequence and structure [5], a novel enzyme's activity cannot yet be predicted from its structure alone [6]. A small, highly conserved constellation of residues in the catalytic site perform the catalytic activity of an enzyme in the active site [7]. The remaining majority of the enzyme structure serves to retain the precise orientation and dynamics of the active site [8].

1.2 Enzyme function and regulation

Enzyme accelerates the rate of chemical reactions in a cell without themselves being altered and without altering the chemical equilibrium between reactants and products. They are crucial for signal transduction and cell regulation, often via protein kinases (PK) and protein phosphatases (PP) [9].

The catalytic activity of enzymes involves the binding of their substrates in a specific interaction to form an enzyme-substrate complex (ES) in the active site. Multiple mechanisms can accelerate the conversion of substrate into the product, which is then released from the enzyme (Figure 1.1).

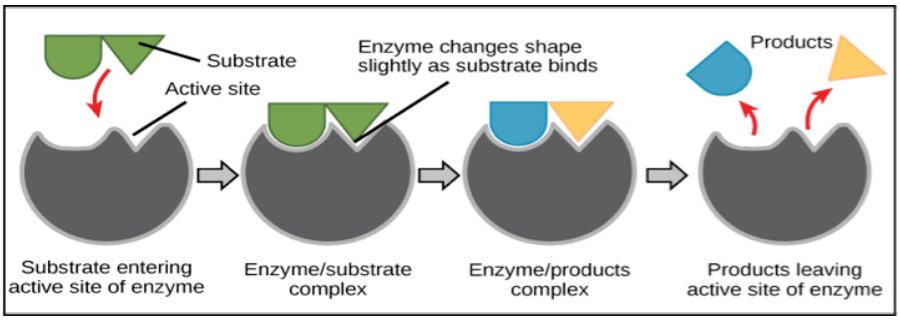

Figure 1.1 Schematic representation of the conversion of substrate into product by an enzyme. Figure reproduced from www.boundless.com.

Enzymes accelerate reactions to approach the transition state by altering the conformation of their substrates, in which the substrate fits precisely into the active site, as illustrated by the lock-and-key model. In many cases, the substrate binding reshape the active site changing the configurations of both the enzyme and substrate which is called induced fit (Figure 1.2).

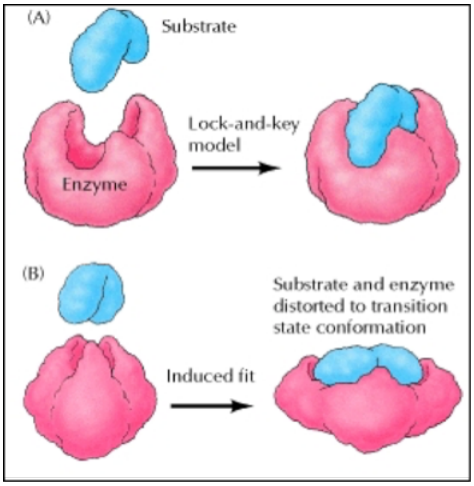

Figure 1.2 Schematic representation of enzyme-substrate interaction. (A) Lock-and-key model, the substrate fits precisely into the active site of the enzyme. (B) Induced-fit model, substrate binding distorts the conformations of both substrate and enzyme(reproduced from Cooper G [10]).

Many enzymes, in addition to binding their substrates, need to be bound to their cofactors, a non-protein chemical compound which is necessary for the biological activity of a protein. Many enzymes bind organic cofactors, such as prosthetic groups, in the active sites that engage in catalysis. For example, heme is a prosthetic group bound to myoglobin and haemoglobin to carry oxygen. In many cases, inorganic cofactors such as metal ions (zinc or iron) are bound to enzymes and play important roles in the catalytic process. In addition, various low-molecular-weight organic molecules called as coenzymes work together with enzymes to increase the rate of enzymatic reactions.

1.3 Regulation of enzyme activity

An important feature of most enzymes is that their activities are not constant but instead can be regulated so that they function appropriately to meet the varied physiological needs that may arise during the life of the cell.

1.3.1 Feedback inhibition mechanism of an enzyme

Feedback inhibition is one common type of enzyme regulation in which the product of a metabolic pathway inhibits the activity of an enzyme involved in the committed step in the pathway. For example, the catecholamines (dopamine, epinephrine and nor epinephrine) are synthesized by a series of reactions starting from the amino acid L-tyrosine (Figure 1.3). The first step in the pathway is catalyzed by the enzyme tyrosine hydroxylase (TH), which is inhibited by catecholamines, the end product of the pathway. Thus, an adequate amount of catecholamine in the cell inhibits TH, blocking further synthesis of catecholamine.

Feedback inhibition may be a result of allosteric regulation, in which enzyme activity is regulated by the binding of small molecules to regulatory sites on the enzyme. The term "allosteric" is derived from Greek word (allo= "other" and steric= "site"), the fact that the regulatory molecules bind to the site other than active site causing the conformational change of the active site and alter the catalytic activity of the enzyme. In the case of, the however, catecholamines bind to the active site, directly coordinating to the iron [11], trapping it in the ferric state, inhibiting the enzyme activity [12].

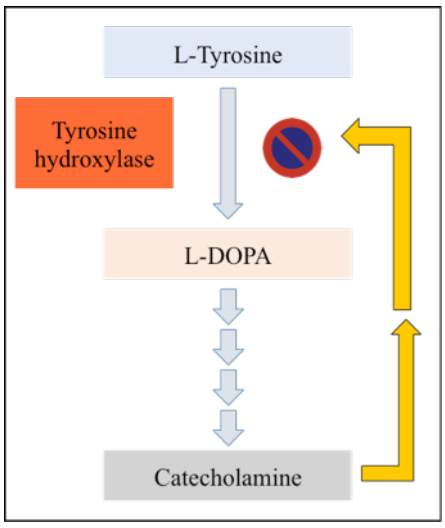

Figure 1.3 Feedback inhibition. The first step in the conversion of L-tyrosine to L-DOPA is catalyzed by the enzyme tyrosine hydroxylase. The activity of this enzyme is inhibited by catecholamine, the end product of the pathway.

1.3.2 Post translational modification (PTM) regulation of an enzyme

PTM refers to enzymatic and covalent modification of one or more amino acid side chains of a given protein. The biological function of a given protein can be altered by PTM even in the absence of changes in the protein level or transcription. PTM reaction not only depends on the spatial orientation of specific amino acid residue (s) but also depends on neighbouring amino acids that allows selectivity and reactivity via affecting the electrophilic nature of the vital amino acid residue that undergoes modification [13]. Examples of PTM and their target amino acids are outlined in the table 1.

Table 1 Examples of post translational modification reaction and their target amino acid residues.

No.	**Amino acid residues (functional reactive group)**	**Types of modification (enzymatic or non-enzymatic)**
1	Serine/threonine (-OH)	Phosphorylation (enzymatic)
2	Cysteine (-SH)	Thiolation (enzymatic), methylation (enzymatic) and oxidative modification (non-enzymatic)
3	Lysine (-ε-NH_2)	Acetylation (enzymatic), biotinylation (enzymatic), hydroxylation (enzymatic)
4	N-terminal of proteins (-α-NH_2)	Prenylation, pyroglutamylation (enzymatic)
5	Glutamine (-$CONH_2$)	Deamination (non-enzymatic)
6	Tyrosine (-OH)	Nitration, sulfation (non-enzymatic), phosphorylation (enzymatic)
7	Methionine (-SCH_3)	Sulfenylation via oxidative modification
8	Tryptophan (indole ring)	Oxidative modification
9	Proline	Hydroxylation (enzymatic)
10	Asparagine	Glycosylation (enzymatic), hydroxylation (enzymatic)
11	Peptide-Lys/Arg-Lys/Arg-peptide	Proteolytic cleavage (enzymatic)
12	Peptide-Gly	C-terminal α-amidation (enzymatic)

1.3.3 Phosphorylation driven regulation of an enzyme

Phosphorylation is one of the most important and relevant PTM, that often regulates the activities of enzymes by covalent addition of phosphate groups to one of the amino acid residues, such as serine, threonine, or tyrosine residues. Such phosphorylation event either stimulates or inhibits the activities of many different enzymes. For example, glycogen is broken down into glucose in response to epinephrine (adrenaline) in muscle cells, thereby providing a source of energy for increased muscular activity. The binding of epinephrine to a receptor on the surface of the muscle cell activates the enzyme glycogen phosphorylase which catalyzes the breakdown of glycogen. Phosphorylation can affect a protein in two important ways.

First, enzyme-catalyzed addition of a phosphate group to a protein may induce a conformational change induced in a protein, because each phosphate group carries two negative charges which can, for example, attract a cluster of positively charged amino acid side chains which, in turn, may change the protein's activity through an allosteric effect by facilitating the binding of ligands elsewhere on the protein surface. This induced conformational change could be reversed by the removal of the phosphate group by a second enzyme (phosphatase).

Second, an addition of phosphate group can provide a structure that can be recognized by the binding sites of other proteins. A small protein domain, known as modules, may provide binding sites for attaching to other protein molecules. For example, phosphorylation of serine residue at position 19 in TH facilitates the binding to 14-3-3 [14]. Therefore, protein phosphorylation and dephosphorylation events may have an important role in impelling the regulated assembly and disassembly of protein complexes.

1.4 Aromatic amino acid hydroxylase family

The enzyme TH, phenylalanine hydroxylase (PAH) and the tryptophan hydroxylases (TPH1 and TPH2) constitute the aromatic amino acid hydroxylase (AAAH) enzyme family. The AAAHs are similar in structure and function, and each enzyme in the family uses molecular oxygen as additional substrate and the cofactor tetrahydrobiopterin (BH_4) to catalyze the incorporation of an –OH group on their aromatic amino acid substrate (Figure 1.4).

Each subunit of the enzyme consists of three domains: an N-terminal regulatory domain, a catalytic domain in the middle and a C-terminal polymerisation domain. Although N-terminal

regulatory domain is flexible and has not been crystallized yet, the C-terminal and catalytic domains have been determined by X-ray crystallography (Figure 1.5). The monomers are very similar in primary structure, especially in the catalytic domain where amino acid substrate is hydroxylated. Human TH is a homotetramer, containing four identical subunits and so are the TPHs, whereas PAH can be a dimer or tetramer [15].

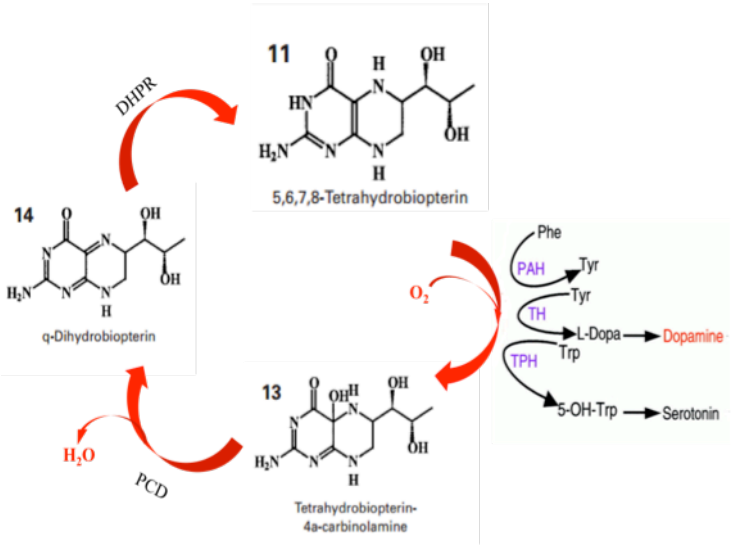

Figure 1.4 The mechanism for the aromatic amino acid hydroxylases including the regeneration of the cofactor tetrahydrobiopterin (BH_4). DHPR = dihydropterin reductase; L-Phe = L-phenylalanine; L-Tyr = L-tyrosine; L-DOPA = L-3,4-dihydroxyphenylalanine; 5-OH-Trp = 5-hydroxytrytophan; PCD = pterin-4a-carbinolamine dehydratase. Figure modified from A.H Németh and B. Thöny [16] and [17].

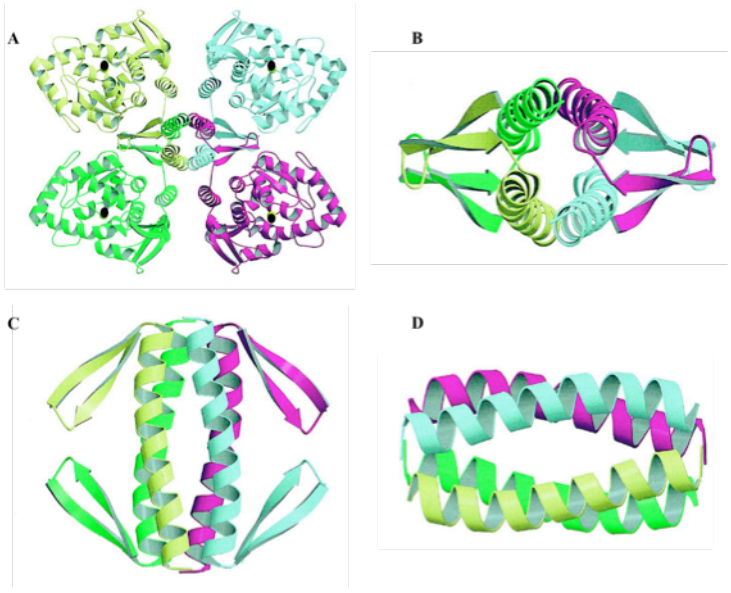

Figure 1.5 Ribbon diagram representation of the tyrosine hydroxylase tetramer. (A) The four subunits are shown in different colour and are related by a crystallographic 222 symmetry. The coiled-coil motif is visible in the centre of each tetramer and the iron bound in the active sites are shown as black spheres. (B) Tetramerization domain shows symmetry. (C) Ninety degree rotation view of tetramerization domain. (D) View of the coiled-coil motif of TH. The crystal structure is determined by X-ray crystallography and found in the protein data bank (PDB; PDB-ID 2xsn).

1.5 Tyrosine hydroxylase and catecholamine synthesis

TH (EC 1.14.16.2) is the rate limiting enzyme that is responsible for catalyzing the conversion of L-tyrosine to L-3,4-dihydroxyphenylalanine (L-DOPA) [18]. TH is a tetrahydrobiopterin (BH_4; cofactor) dependent enzyme that utilizes molecular oxygen as well as iron to catalyze the reaction (Figure 1.8). L-DOPA is a precursor for dopamine, which, in turn, is a precursor for other important catecholamine neurotransmitters norepinephrine (noradrenaline) and epinephrine (adrenaline). Figure 1.9 shows the biosynthetic pathway of catecholamines.

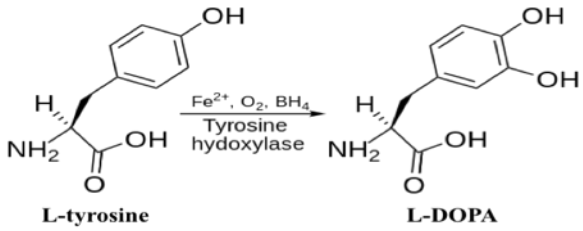

Figure 1.6 Tyrosine hydroxylase catalyzes the conversion of L-tyrosine to L-DOPA by hydroxylation in the meta position of L-tyrosine using Fe^{2+}, O_2 and BH_4.

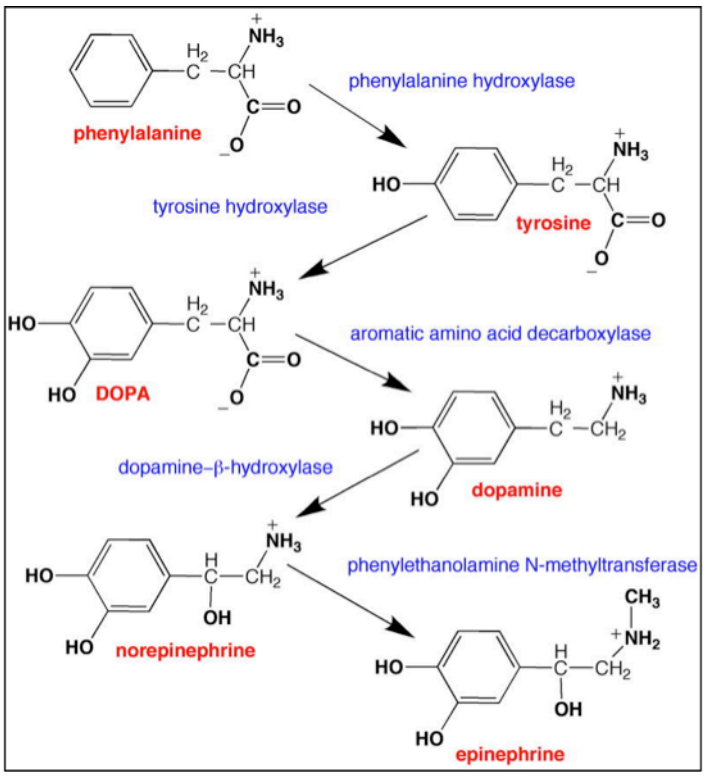

Figure 1.7 Catecholamine biosynthetic pathway. Phenylalanine hydroxylase converts phenylalanine to tyrosine; tyrosine is converted to L-DOPA by tyrosine hydroxylase. Aromatic amino acid decarboxylase converts DOPA into dopamine. Dopamine is hydroxylated to norepinephrine by dopamine-β-hydroxylase, which is methylated to epinephrine by phenylethanolamine N-methyltransferase. Tyrosine hydroxylase is the rate-limiting enzyme of the pathway (reproduced from Daubner SC [19]).

In humans, TH presents several isoforms due to alternative splicing where isoforms 1 to 4 (hTH1-hTH4) are most abundant [20]. hTH1, which is very similar to rat and mouse TH in length and sequence, is the major isoform in brain and peripheral tissues and is also the most studied human isoform *in situ* and *in vitro*.

TH is a homotetramer with a molar mass of ~240 kDa [21]. Each subunit comprises of three domains, the C-terminal arm consisting of two β-strands and a 40 Å long α-helix form a tetramerization domain (Figure 1.6) [15, 22]. The central catalytic core is made up of ~300 amino acids[23], in which all necessary residues for catalysis are positioned, along with a non-covalently bound Fe^{3+}[24] which is held in place by two histidines (331 and 336) and a glutamate (376), making it a non-heme, non-iron-sulfur iron-containing enzyme[23, 25]. The N-terminal regulatory domain consists of ~160 amino acids make up a regulatory domain, which may control the access of substrates to the active site[19].

The synthesis of catecholamines is highly controlled by transcriptional and translational mechanisms. However posttranslational modifications, notably phosphorylation at different N-terminal residues, as well as other short-term effects such as binding to 14-3-3 proteins, feedback inhibition by catecholamines and substrate inhibition further regulate TH activity and localization [19]. Different kinases are responsible for the phosphorylation of the enzyme at Thr8, Ser19, Ser31 and Ser40 N terminal residues[19]. Little is known about the possible effects of phosphorylation at Ser/Thr8[26]. TH phosphorylated at Ser40 by the cAMP-dependent protein kinase (protein kinase A; PKA) is less susceptible to feedback inhibition by catecholamines [27, 28]. TH is phosphorylated at Ser31 by extracellular regulated kinases 1and 2(ERK1 and ERK2)[29]. It is well established that phosphorylation at Ser31 and Ser40 (THpSer31 and THpSer40,respectively) leads to an increase of TH activity for the purified protein as well as in catecholamine producing cells[18, 29-32].TH is phosphorylated at Ser19 and to a lesser extent at Ser40 by the calcium-calmodulin-dependent protein kinase (CaMPKII) [33, 34]. Other kinases like mitogen-activated-protein kinase-activating protein kinase (MAPKAPK2) [35] and p38 regulated/activated kinase (PRAK) [36] were subsequently found to phosphorylated Ser19. Although, the direct involvement of Ser19 phosphorylation in TH activity is unknown, TH phosphorylated at Ser19 increase the TH activity through a mechanism that involves the binding to the 14-3-3 proteins [31].

Catecholamine neurotransmission disturbances are hallmarks of many neuropsychiatric and neurodegenerative disorders such as Parkinson's disease (PD), L-dopa-responsive dystonia

and tyrosine hydroxylase deficiency (THD) [37-39], all of which currently lack good long-term treatments.

1.6 The 14-3-3 proteins

The 14-3-3 protein family was first identified and named in 1968 by Moore *et al* after the migration positions of the proteins in ion exchange chromatography and starch gel electrophoresis [40]. There are several isoforms of the 14-3-3 family that show high sequence identity, >50% amino acid identity both within and across species [41], and almost identical overall structure, thus the proteins are highly conserved.

14-3-3s exist as dimers in their native state [42], and it has been shown that the proteins can form both homo- and heterodimers [43]. Each monomer has an average molecular weight of ~30 kDa with an acidic isoelectric point of ~4.5. Crystallographic studies of 14-3-3 showed that the protein has a cup shaped structure with nine anti-parallel helices designated αA-αI [44, 45], where C-terminal form its walls and the N-terminal helices of the two subunits forms the groove of the dimer (Figure 1.8). The inner phosphopeptide-binding pocket is the most highly conserved region [43]. The binding grove exhibits amphipathic features, as one side of the groove consists of hydrophobic residues, whereas the other side presents charged and polar residues.

The proteins may have a fundamental importance as they are ubiquitously expressed in all eukaryotic cells [43, 46]. However, the number of different isoforms varies from species to species ranging from 2 in the nematode *Caenorhabditis elegans*to 12 in the plant *Arabidopsis*. In humans, 14-3-3 protein family consists of seven known isoforms, named β, γ, ε, ζ, η, σ, and τ/θ after their elution profile on reverse-phase high performance liquid chromatography [31]. The phosphorylated form of β and ζ were initially designated as α and δ, respectively [47].

The ubiquity of the 14-3-3 proteins and the high degree of conservation suggest a fundamental importance in the eukaryotic cell [46]. Accordingly, with over 500 binding partners [48, 49] and seven human isoforms, it is not surprising that the 14-3-3 protein family is said to be involved in nearly all cellular processes [50]. These processes are, for e.g, transcription, regulation of cell cycle, intracellular trafficking and targeting, cytoskeletal structure and transcription [40], and the proteins are key regulators of numerous processes, ranging from mitosis to apoptosis [51].

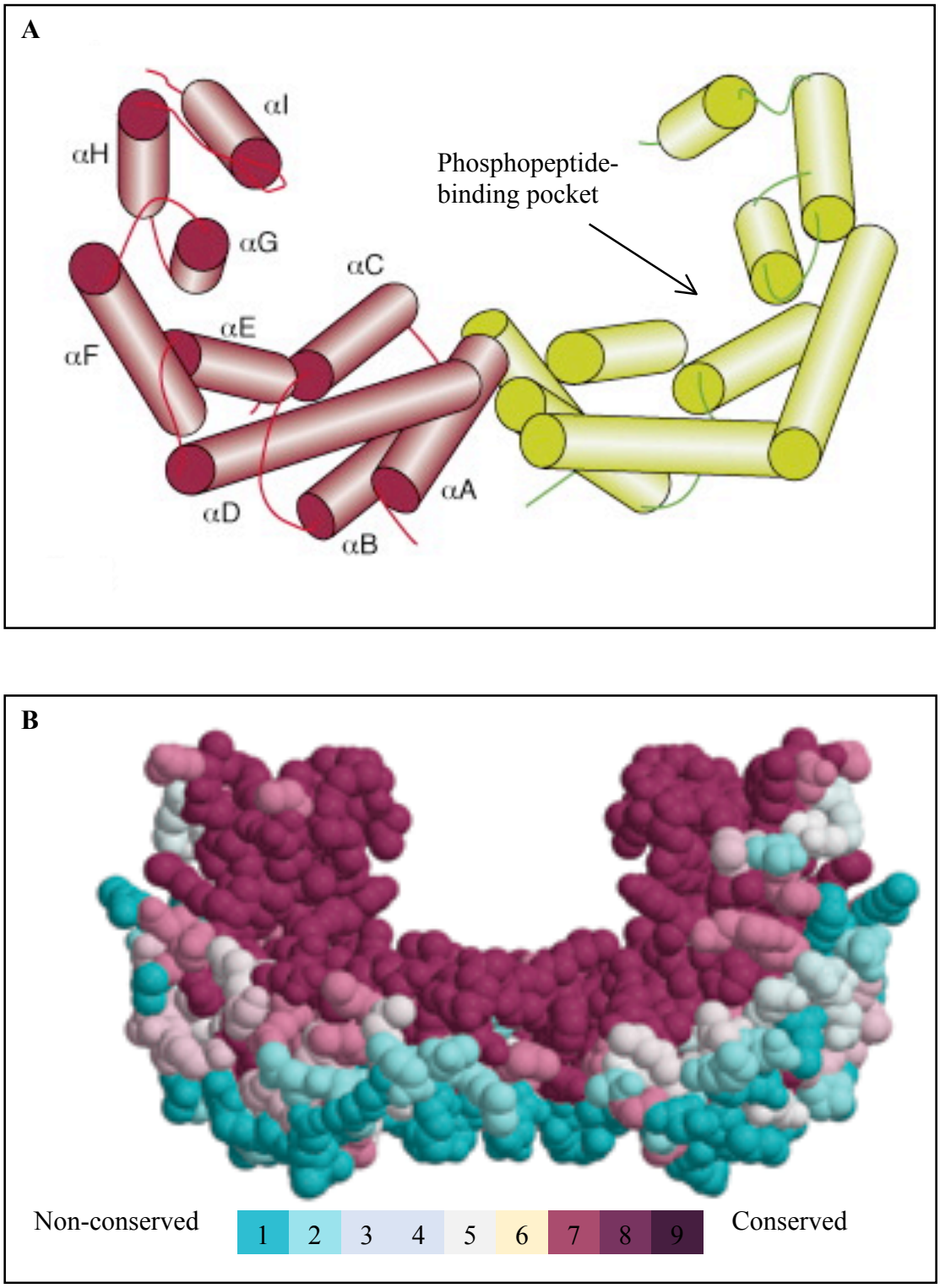

Figure 1.8 The structure of 14-3-3. A: The structure of 14-3-3γ where the helices αA-αI are shown as cylinders (figure is reproduced from Maria Zannis-Hadjopouloset al.[52]). B: Structure of 14-3-3ζ shaded according to residue conservation (figure is reproduced from Bridges, D and G.B Moorhead [43]).

Phosphorylation of TH by PKA at Ser40 and by Erk 1 and 2 at Ser-31 results in a direct increase in its enzymatic activity. However, the activation of TH by CaM kinase II [53, 54] requires an additional protein factor, which is now know as the 14-3-3 protein [31, 55].

Accumulating evidence suggests that TH is directly activated by PKA without 14-3-3 and the stimulatory effect of PKA is an addition to the effect of CaM kinase II plus 14-3-3 [56]. On the other hand, it has been shown that the yeast 14-3-3 protein isoform (BMH1) can bind to all four human TH isoforms phosphorylated only at Ser40with high affinity [57]. It is unknown the reason why yeast 14-3-3 protein isoforms bind to TH phosphorylated at Ser40 but not mammalian [57].

The 14-3-3 protein family is involved in many cellular functions, mostly via subcellular sequestration and scaffolding of binding partners proteins in a serine/threonine-phosphorylation dependent manner [58] (Figure 1.9). Although, the seven isoform of 14-3-3 proteins have high sequence identity and are all cytosolic, they do have specific subcellular localization preferences [31, 56]. Thus, TH own cellular localization is expected to be modulated depending to which 14-3-3 it associates with. In this line, 14-3-3ζ has been suggested to associate with mitochondria [59] and actually THpSer19, when interacting with 14-3-3ζ, localizes to the mitochondria [60] pointing to this important organelle as a novel L-DOPA/dopamine synthesis site. In neurology and neurodegeneration, in relation to the dopaminergic system, down-regulation of 14-3-3 is associated with decreased TH levels and dopamine synthesis [61].

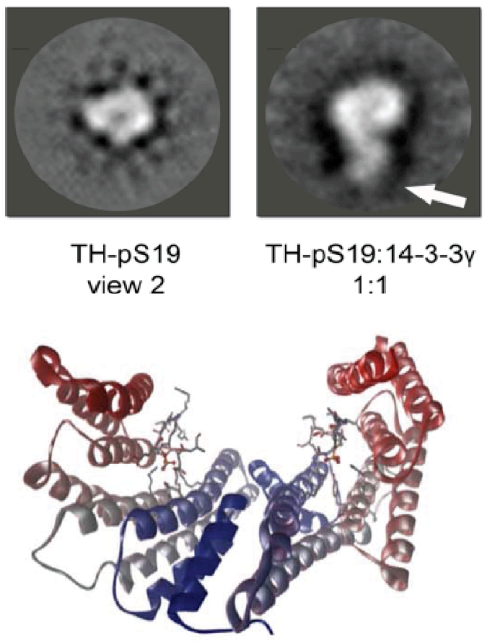

Figure 1.9 Structural analysis of THpS19 and the THpS19:14-3-3 complex by cryo-EM (upper panel, figure is reproduced from Kleppe R et al [14]). 3D-structure of 14-3-3 with bound N-terminal region of THpSer19 (lower panel).

1.7 Aim of the project

The main purpose of this project is to gain insight into the cellular role of Serine 19 phosphorylation in tyrosine hydroxylase. The project is subdivided into the following key objectives:

1. To create the phospho-null and phospho-mimicking mutants of THpSer19 by site-directed mutagenesis to study the function of Ser19 phosphorylation in TH.

2. To investigate the oligomeric state of TH in the subcellular fractions (nuclear and cytosolic) of neuroblastoma cells.

3. To study the cellular distribution of endogenous TH and to investigate the effect of phosphorylation in the subcellular localization of TH by expressing V5-TH mutants in neuroblastoma cells.

4. To examine the co-distribution of TH and 14-3-3 proteins and to investigate the interaction of THpSer19 and 14-3-3 proteins in the nucleus of neuroblastoma cells.

2. THEORETICAL AND METHODOLOGICAL CONSIDERATIONS

2.1 V5-TH construct

The coding sequence of human tyrosine hydroxylase isoform 1 (hTH1) was cloned into the mammalian expression vector pcDNA™6.2/nTC-Tag-Dest (Invitrogen). This construct was readily available in the laboratory at the start of this Master project will be referred to as V5-TH throughout this report.

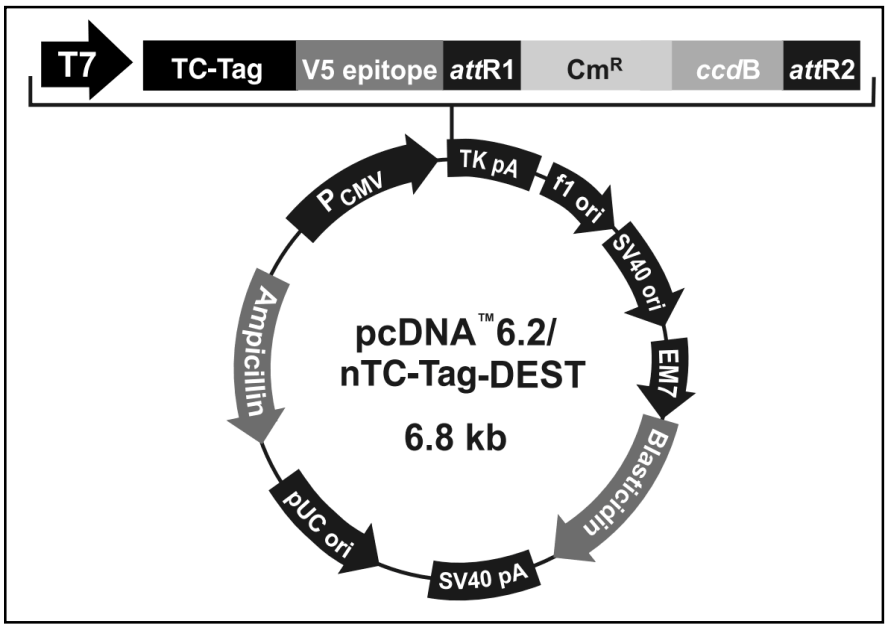

Figure 2.1 Map of pcDNA™6.2/nTC-Tag-Dest plasmid vector. The *h*TH1 gene is cloned into the vector in attR1 region.

The pcDNA™6.2/nTC-Tag-DEST vector contains human cytomegalovirus immediate-early (CMV) promoter/enhancer for high-level expression in a wide range of mammalian cells. The Herpes Simplex Virus thymidine kinase polyadenylation signal (TK pA) allows efficient transcription and polyadenylation of the recombinant transcript. The vector presents two different tags N-terminal of the coding sequence. The first one is a tetracysteine tag (TC-Tag) that allows fluorescence detection using biarsenic compounds. The second tag is a V5 epitope that can be used for a wide range of applications based on the use of the highly specific and sensitive antibodies generated towards this epitome. In this project we have used it mainly for Western blotting. SV40 early promoter and origin allows efficient, high-level expression of the blasticidin resistance gene that can be used for the selection of stable transfectants in mammalian cell lines. The pUC origin allows high copy replication and maintenance of the

plasmid in E. coli and the ampicillin resistance gene allows the selection of transformants in *E. coli*.

2.2 Site-directed mutagenesis

Site directed mutagenesis (SDM) is a useful technique that allows to introduce specific mutations into plasmids in a controlled manner in order to obtain a protein with substituted, deleted or inserted amino acids. Briefly, the process is based on the amplification of the target plasmid using the polymerase chain reaction (PCR) methods and a pair of complimentary oligonucleotide primers (forward/reverse) bearing the desired mutation/s.

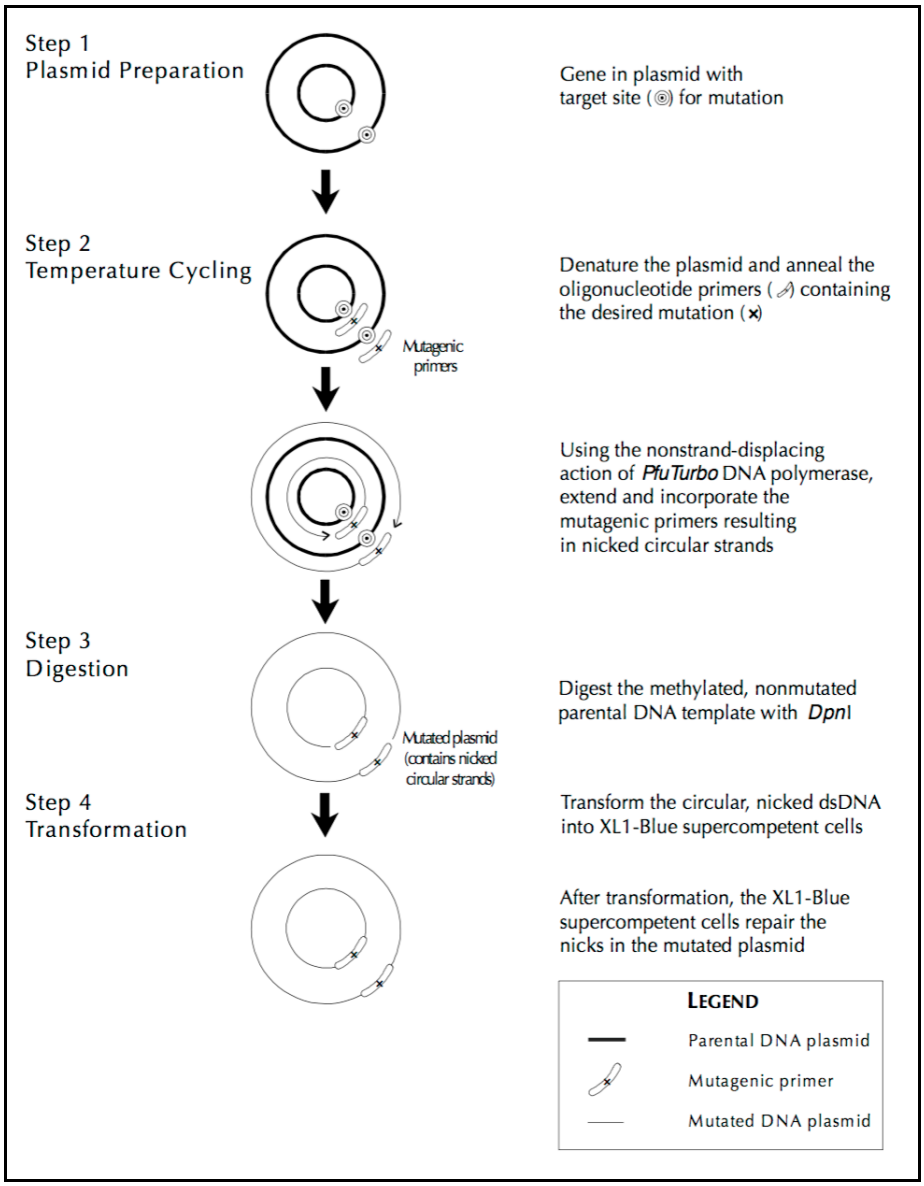

Figure 2.2 Mutagenesis using QuickChange® site-directed mutagenesis kit from Stratagene (www.stratagene.com). In this work XL10-Gold® was used, instead of *Epicurian Coli* XL1-Blue®.

A crucial aspect to consider when designing primers is the length and melting temperature, to ensure good base-pairing with DNA strand. During the PCR the plasmid is denatured first, so that the primers can anneal to the DNA strands. Throughout the thermocycling reactions, primers are extended by a polymerase (*Pfu* DNA polymerase was used during this project) producing copies of plasmid containing the desired mutation (Figure 2.2, step 2). The system takes advantage of the fact that the plasmid propagated and isolated from *E.*coli is methylated, but the one synthesized by the PCR is not and uses an endonuclease (*DpnI*) which selectively digests methylated DNA to remove the non-mutated template plasmid from the PCR products(Figure 2.2, step 4). The plasmids containing mutated DNA are then transformed into competent XL-gold bacteria for their propagation and subsequent purification. In the case of this project we used a commercial alkaline lysis kit (QIAGEN® plasmid DNA purification Mini-prep kit) followed by binding of plasmid DNA to QIAGEN resin under appropriate low-salt and pH conditions. RNA, proteins, and low-molecular–weight impurities are removed by a medium-salt wash. Plasmid DNA is eluted in a nuclease free water. The plasmids isolated from *E.coli* were sequenced in both directions to verify the mutations.

2.3 Sequencing

DNA sequencing is the most important tool in molecular biology to determine the precise order of nucleotides within a segment of DNA. The most widely used technique, chain-termination method, developed by Sanger and Coulson, which relies on the enzymatic synthesis of DNA *in vitro* in the presence of chain-terminating inhibitors[62].

Similar to PCR, the sequencing reaction is initiated by double strand denaturation of a template DNA followed by annealing a short oligoneucleotide primer on to the temple to be sequenced. The chain extension is initiated by addition of polymerase along with deoxyribonucleoside triphosphates (dNTPs). In addition, dye-labelled dideoxyribonucleoside triphosphates (ddNTPs), in which 3'-hydroxyl has been replaced by a hydrogen, are used which can be incorporated just as efficiently as the normal nucleotides into the growing polynucleotide strand, but will block further strand synthesis. The final products of the sequencing reaction consist of3’end fluorescently labelled fragments of different lengths. These products can be separated electrophoretically on a polyacrylamide gel, even if they differ by only one base pair.

Different fluorescent dye attached to each of the ddNTPs, when excited by a laser emit a distinct colour of light at a different wavelength. The resulting fluorescence can be detected by a charge-coupled camera (CCD) and translated into a chromatogram.

2.4 Electrophoresis

Electrophoresis is a technique mainly used to separate and purify macromolecules, especially proteins and nucleic acids that differ in size, charge or conformation in presence of an electric field.

2.4.1 Clear-native PAGE

Clear-native PAGE is used to separate acidic water-soluble and membrane proteins, in an acrylamide gradient gel in non-denaturing conditions [63]. As no charged dye is used to impose negative charge, the electrophoretic separation of proteins depends on the intrinsic charge of the proteins. This technique implies the usage of non-ionic detergent for the solublization of biological membrane and separation of attached proteins, for this project NP-40 is used. Following the solubilisation, the proteins are electrophoretically separated and the migration distance depends on the protein's intrinsic charge and the pore size of acrylamide gradient gel. The separated protein complexes are electroblotted onto PVDF membrane and immuno-detected, for this work, by the antibody specific to V5 epitope.

2.4.2 Blue-native PAGE

Blue-native PAGE (BN-PAGE)is the technique used to isolate native protein complexes electrophoretically by imposing negative charge on to the protein sample [64]. It was initially developed for the separation of mitochondrial membrane proteins [65]. As mentioned above in CN-PAGE, non-ionic mild detergent is used for solublization of biological membrane. Following solubilization, water soluble anionic dye Coomassie blue G-250 is added which imposes a charge shift on the proteins that causes even basic proteins to migrate to the anode at pH 7.5 during BN-PAGE[66]. Thus, proteins are separated according to the size in acrylamide gradient gels as protein migration gradually decelerates with decreasing pore size of the gradient gel. To ensure the entrapment of separated protein throughout the electrophoretic separation, blue anionic cathode buffer is used. The separated protein complexes can be electroblotted onto PVDF membrane and immuno-detected as we have done in this project.

2.4.3 SDS-PAGE

Sodium dodecylsulfate polyacrylamide gel electrophoresis (SDS-PAGE) is common method for separating proteins based on their molecular weight using a discontinuous polyacrylamide gel as a support medium and sodium dodecyl sulfate (SDS) to denature the proteins, an anionic detergent which binds to the polypeptide backbone and stabilises unfolded conformations of the polypeptide chains due to the negative charges of the bound SDS. It also dissolves salt-bridges and other stabilising intra-proteins interactions. The amount of SDS bound to polypeptide is in proportion to its relative molecular mass. In addition to SDS, reducing agents such as dithiothreitol (DTT) or 2-mercaptoethanol (beta-mercaptoethanol/BME) are routinely used together with heating the sample to near boiling point, to further denature the proteins by reducing disulfide linkage and thus breaking the quaternary protein structure.

During the electrophoresisseparation, negatively charged polypeptide-SDS migrates toward the anode (positive electrode). Larger molecules are restrained from migrating as fast as smaller molecules by the polyacrylamide gel matrix because the charge-to-mass ratio is nearly the same among SDS-denatured polypeptides. The final separation of proteins is dependent almost entirely on the differences in relative molecular mass of polypeptides.

2.5 Western blot

The western blot (also known as immunoblot) is a widely accepted analytical technique used in various molecular biology disciplines to detect specific proteins in given sample. It uses polyacrylamide gel to electrophoretically separated protein samples, for example; native proteins or denatured proteins by the length of the polypeptide. The separated protein samples are then transferred or blotted onto a matrix (nitrocellulose or PVDF membrane). The membranes are blocked with dilute solution of protein (BSA or non-fat dry milk) to prevent interaction between antibody and membrane. The sample proteins are then detected either directly (target protein is detected by primary antibody which is conjugated to label molecule, such as biotin, an enzyme or a fluorescent dye) or indirectly (target protein is detected by primary antibody which is inturn is detected by secondary antibody which is conjugated to label molecule), for this project indirect method was used. Labelled probe bound to the target protein is detected by various detection methods. For this project enhanced chemiluminescence (ECL) detection method was used; a technique in which horseradish peroxidase enzyme (HRP) is conjugated to an antibody that specifically recognizes the

molecule of interest. The enzyme complex catalyzes the conversion of chemiluminescent substrate (an organic dye such as luminol) into sensitized reagent, which produces excited intermediates upon oxidation by a strong oxidizing agent (hydrogen peroxide). These excited intermediates emit light when it decays to a lower energy level and return to their stable ground state.

2.6 Immunofluorescence

Immunofluorescence (IF) is a common laboratory technique used to detect a target protein by a specific antibody and is visualized using fluorescence microscopy, allowing visualisation of the distribution of the target molecule within the cell. There are two main methods of immunofluorescent labelling, direct and indirect. Direct Immunofluorescence uses an antibody chemically conjugated to fluorophore specific to the molecule of interest and can be detected via fluorescent microscope. For this work, indirect immunofluorescence technique was used, whereby the antibody specific for target molecule (called the primary antibody) is unlabeled, and a second anti-immunoglobulin antibody directed toward the constant portion of the first antibody (called the secondary antibody) is tagged with the fluorescent dye and can be detected using fluorescent microscope.

Usually for this method cells are grown on glass coverslips and are fixed using paraformaldehyde. Then if the target protein is intracellular, samples are permeabilized using mild detergent such as triton. In order to blot out unspecific antibody binding, samples are blocked with serum before primary antibody incubation. Excess antibody is washed before incubation with the secondary antibody that will recognize the primary antibody. Again antibody excess is washed and cells are also washed briefly with water to avoid salt crystals in the sample. Finally samples are mounted using specific mounting media for microscopy to ensure the best results. In this project we used Prolong gold which has DAPI to stain nucleus.

We used antibody in combination with stains, that can recognize laminin β1 (a glycoprotein) present on a nuclear envelope to detected nuclear structure. In order to analyze the immunofluorescence samples, the epifluorescence microscope and the confocal microscope is widely used or various super-resolution microscope designs that are capable of much higher resolution can also be used. In this project we have used confocal microscopy to visualize our samples and the principles it is based upon are described in section 2.8.

2.7 Proximity ligation assay

Proximity ligation assay (PLA), a the method based on the simultaneous and proximate identification of target molecules by pairs of affinity probes, giving rise to an amplifiable detection signal [67]. The protein(s) of interest is detected by two primary antibodies raised in different species (Figure 2.3, step 1). Species-specific secondary antibodies conjugated with a unique short oligonucleotide, called PLA probes (Plus and minus), bind to the primary antibodies (Figure 2.3, step 2). In close proximity the oligonucleotides will hybridize (Figure 2.3, step 3) to the two PLA probes and join in circle-forming DNA oligonucleotides by enzymatic ligation (Figure 2.3, step 4). Nucleotides and fluorescently labelled oligonucleotides are added together with a DNA polymerase and by using the ligated circle as a template, the oligonucleotide arm of one of the PLA probes acts as a primer for a rolling-circle amplification (RCA, Figure 2.3, step 5) reaction, producing a concatemeric product. A distinct fluorescent spot is generated by hybridization of fluorescently labelled oligonucleotides to the RCA product and the signal is easily detected by fluorescence microscope (Figure 2.3, step 6). Various application of the assay includes detection and quantify protein:protein interaction, posttranslational modification and protein expression.

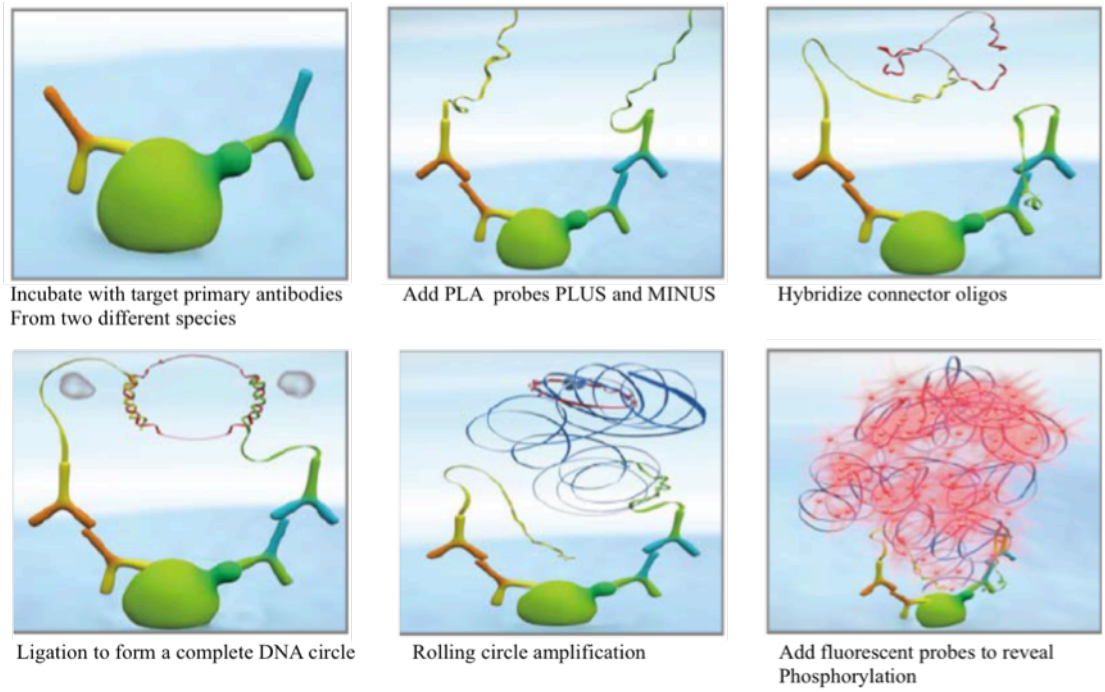

Figure 2.3 schematic presentation of principle of in situ PLA [68].

2.8 Confocal microscopy

Confocal microscopy is an optical imaging technique that increases optical resolution as well as contrast of a micrograph by addition of a spatial pinhole placed at the confocal plane of the lens to eliminate out-of-focus light. It is a combination of conventional light microscope and fluorescent microscope which allows analysis of fluorescent labelled specimens without physical sectioning. Excess illumination of a sample and quick bleaching of the fluorescent signal are reduced, since images are obtained by scanning. Fluorescent is a property of certain chemical substances that has ability to illuminate with high intensity at a specific wavelength when excited by shorter wavelength. To achieve a high resolution, one or more laser lights are focussed across the sample which then illuminates to produce optical section of the whole sample and eliminate "out-of-focus" light with the use of pinhole airy. At each point some parts of the sample will get excited and emit light of a lower wavelength, for example, when green light is used for excitation, red light is emitted (Figure 2.4). The reflected light is deviated and emitted light is passed through dichromatic mirror and detected by photo-detector, recorded and displayed as digitalized images. It is possible to link morphology and cellular function by tridimensional reconstruction (XYZ) and time-analysis (XYT) [69].

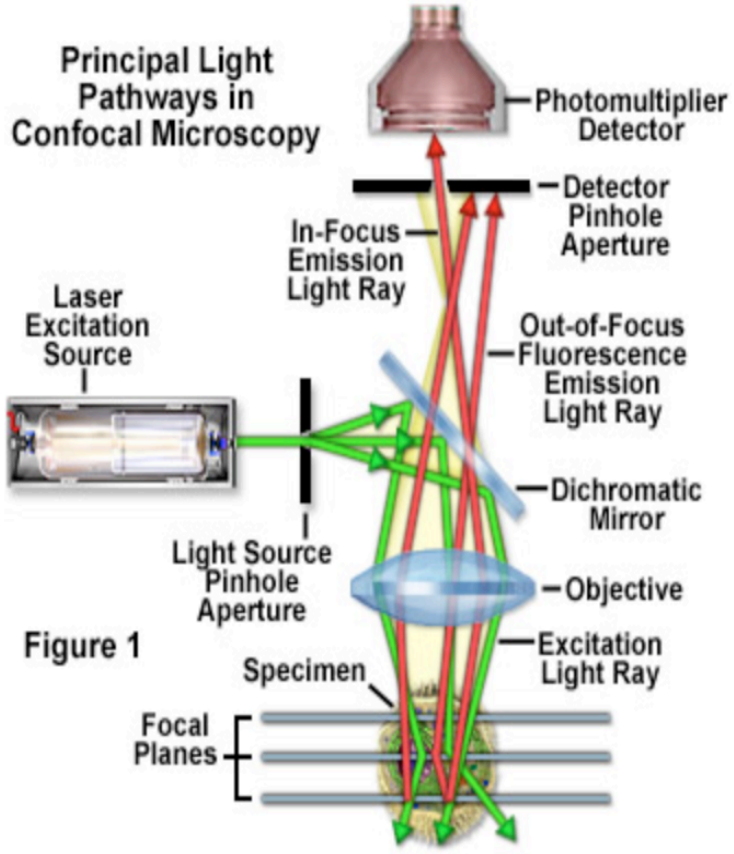

Figure 2.4 Schematic representation of the principle of confocal microscopy [70].

Resolution for a 63x oil immersion objective with numerical aperture 1.4 is 0.2 µm for green light. Oil immersion is to avoid a refraction and therefore loss of information at the interface of two media. Since objectives with a high numerical aperture have a limited depth of field due to their high magnification, sample is easily moved out of focus. 3-D pictures can be obtained by moving the sample through the focal plane of the lenses.

3. MATERIALS

3.1 Instruments

Method	Instrument	Provider
PCR	Master Cycler gradient	Eppendorf
Concentration measurements	Nanodrop ND-1000	Saveen Werner
Concentration measurements	Direct Detect™	Millipore
Centrifugation	Centrifuge 5417 R, 5810 R	Eppendorf
Ultra-centrifugation	Optima max-130K	Beckman
Cell culture (incubator)	Heraeus Hera Cell 150	Tamro Medlab
Bacterial culture	Excella E24 Incubator Shaker	New Brunswick scientific
Cell counting	Scepter handheld automated Cell counter	Millipore
Electrophoresis	Mini-PROTEAN® electrophoresis system	Bio-Rad
Electro blotting	Trans-Blot® Turbo™ Transfer System	Bio-Rad
Confocal microscopy	TCS SP5 resonant scanner	Leica Microsystems
Chemiluminescence	ChemiDoc™ XRS+ System	Bio-Rad

3.2 Enzymes

Name	Provide
Pfu Turbo® DNA polymerase	QuickChange
DpnI restriction enzyme	QuickChange
DNase I RNase free	Thermo-Scientific
Trypsin	Sigma-Aldrich

3.3 Cell lines and bacteria

Name	Provider
HEK293 (Human embryonic kidney cell line)	ATCC
SH-SY5Y	ATCC
Escherichia coli XL10-Gold ultracompetent cells	Stratagene

3.4 Medium and cell equipment

Name	Provider
Dulbecco's modified Eagle's medium (DMEM)	Sigma-Aldrich
Fetal bovine serum (FBS)	Sigma-Aldrich
Opti-MEM® reduced serum media	Gibco
P100 cell culture dish	Nunc
P60 cell culture dish	Nunc
4-well plates	Nunc

3.5 Chemicals

Name	Provider
1,4-dithiothreitol (DTT)	Sigma-Aldrich
4',6-diamidino-2-phenylindole (DAPI)	ThermoFischer
4, hydroxycinnamic acid (Enhancer)	Sigma
5-amino-2,3-dihydro-1,4-phthalazinedione (Luminol)	Sigma
Acetic acid (CH_3COOH)	Sigma-Aldrich
Acrylamide 30%	Bio-rad
Agar-agar	Merck
Ammonium persulfate (APS)	Bio-rad
Ammonium sulphate ($(NH_4)_2SO_4$)	Sigma-Aldrich
Bromophenol blue	Merk
Collagen	Advanced BioMatrix
Coomassie brilliant blue G-250	Serva
Deoxynucleotriphosphates mix (dNTPs)	Invitrogen
Dimethyl sulfoxide (DMSO)	Sigma-Aldrich
Ethanol	Sigma-Aldrich
Ethylenediaminetetraacetic acid (EDTA)	Thermo-Scientific
Glucose	Sigma-Aldrich
Glutamine (Gln)	Sigma-Aldrich
Glycerol	GE healthcare
Glycine	Sigma-Aldrich
Guanidine hydrochloride (GuHCl)	Sigma
Hydrogen chloride (HCl)	Merck
Hydrogen peroxide (H_2O_2)	Merck
Isopropanol	Sigma-Aldrich
Kanamycin	Sigma-Aldrich
Laminin	Sigma
Magnesium Chloride ($MgCl_2$)	Merck
Methanol	Sigma-Aldrich
Monopotassium phosphate (KH_2PO_4)	Sigma
Paraformaldehyde (PFA)	Fluka
Phosphate buffer saline (PBS) tablet	Sigma-Aldrich
Phosphatase inhibitor tablet	Roche

Potassium Chloride (KCl)	Sigma
Protease inhibitor tablet	Roche
Sodium chloride (NaCl)	Sigma-Aldrich
Sodium dodecyl sulphate (SDS)	Sigma-Aldrich
Sodium hydrogen phosphate (Na_2HPO_4)	Sigma
Tetramethylethylenediamine (TEMED)	Bio-Rad
Trizma base (Tris-HCl)	Sigma-Aldrich
Sucrose	Sigma-Aldrich
Trypsin	Sigma-Aldrich
Tryptone	Sigma-Aldrich
Triton X-100	Sigma
Tween 20	Sigma-Aldrich
Yeast extract	Merck

3.6 Antibodies

Name	Provider
Mouse anti-V5	Life Technologies
Mouse anti-total TH	Santa Cruz
Rabbit anti-total TH	Thermo-Scientific
Rabbit anti-THpS19	Phosphosolutions
Rabbit anti-laminin β	Abcam
Rabbit anti-pan 14-3-3	Santa Cruz
Rabbit anti-14-3-3 γ	IBL America
Goat anti-rabbit HRP	Santa Cruz
Goat anti-mouse HRP	Santa Cruz
Goat anti-rabbit Alexa fluor 488	Invitrogen
Donkey anti-rabbit Alexa fluor 647	Invitrogen
Goat anti-mouse Alexa fluor 555	Invitrogen

3.7 Other products

Name	Provider
pcDNA™6.2/nTC-Tag-Dest plasmid	Life Technologies
Quick change mutagenesis kit	Stratagene
Plasmid extraction miniprep kit	Qiagen
Plasmid extraction midiprep kit	Qiagen
Duolink Insitu reagents	Olink Bioscience
BigDye sequencing kit	Thermo Scientific

3.8 Buffers and solutions

3.8.1 Complete Dulbecco's modified Eagle's medium

Final concentration	Chemical	Initial concentration	Volume
-	DMEM	-	500 ml
10% (v/v)	FBS	100 %	50 ml
2mM	Glutamine	226 mM	5 ml

New glutamine was added every 4 weeks to prevent a lower concentration due to deamination. 1 x PBS was prepared by adding 1 PBS tablet (Sigma-Aldrich) in 200 ml distilled water

3.8.2 SDS-PAGE gels

Substances	Running gel (10%)	Stacking gel (4%)
30% acrylamide	3 ml	650 µl
H_2O	4.4 ml	3.05 µl
1.5 M Tris-HCl pH 8.8	2.5 ml	-
0.5 M Tris-HCl pH 6.8	-	1.25 ml
10% SDS	100 µl	50 µl
10% APS	50 µl	25 µl
TEMED	5 µl	5 µl

3.8.3 SDS-PAGE running buffer 10 X

Concentration	Chemical	M.W (g/mol)	For 1 L
248 mM	Tris	121.14	30 g
1.92 M	Glycine	75.06	144 g
1% w/v	SDS	288.372	10 g

Dilute to 1X for running SDS-PAGE gels.

3.8.4 SDS denaturing buffer 4 X

Concentration	Chemical	M.W (g/mol)	For 10 ml
250 mM	Tris-HCl pH6.8	121.14	0.30 g
8% (w/v)	SDS	288.372	0.8 g
40% (v/v)	Glycerol	92.09	4 ml
0.02%	Bromophenol blue	669.96	0.002 g

Final concentration of 1mM DTT was added into the sample before loading into the gel.

3.8.5 Luria-Bertani (LB) medium

Concentration	Chemical	M.W (g/mol)	For 1 l
10g/l	Tryptone	-	10 g
5g/l	Yeast extract	-	5 g
171 mM	NaCl	58.44	10 g

LB medium was autoclaved after the components were mixed.

3.8.6 Super optimal broth with catabolic repression (SOC) medium

Concentration	Chemical	Initial concentration	For 1 L
2% (w/v)	Tryptone	-	20 g
0.5% (w/v)	Yeast extract	-	5 g
0.05% (w/v)	NaCl	58.44 g/mol	0.5 g
1 M	KCl	4 M stock	250 ml
10 mM	$MgCl_2$	10 M stock	1 ml
20 mM	Glucose	10 M stock	2 ml

All components, except for the magnesium chloride and the glucose were mixed and the medium was autoclaved. Sterile magnesium chloride and glucose was added right before use.

3.8.7 Native PAGE buffers

Native PAGE running buffer

50 mM BisTris

50 mM Tricine

pH adjusted to 6.8

Anode buffer

50 ml Native PAGE running buffer 20X

950 ml deionized water

Cathode buffer light blue

10 ml Native PAGE running buffer 20X

1 ml Native PAGE cathode additive 20X

189 ml deionized water

3.8.8 Destaining solution

Final concentration	Chemical	Initial concentration	For 1 L
10% (v/v)	EtOH	Absolute	100 ml
10% (v/v)	Acetic acid	99.8%	100 ml
-	Water	-	800 ml

3.8.9 Native transfer buffer

Concentration	Chemical	M.W (g/mol)	For 1 L
12mM	Trizma base	121.14 g/mol	1.45 g
96 mM	Glycine	75.06 g/mol	7.2 g
0.1% (v/v)	SDS	288.372	1 g

4. METHODS

4.1 Site directed mutagenesis

In order to introduce the TH-S19A and TH-S19E specific mutations, site-directed mutagenesis was performed using Quickchange™Site-Directed mutagenesis Kit from Stratagene® following the manufacturer's instructions.

4.1.1 Primer design

The oligonucleotide primers used to obtain TH-S19A and TH-S9E mutants from the V5-TH wild type vector were designed using PrimerX (www.bioiformatics.org/primerx) and their sequences are shown in Table 1.

Primer	Sequence*	Length (nt)
TH-S19A-F	5'-CTTCCGCAGGGCCGTG**G**C**G**GAGCTGGACGCCAAGC-3'	35
TH-S19A-R	5'-GCTTGGCGTCCAGCTC**C**G**C**CACGGCCCTGCGGAAG-3'	35
TH-S19E-F	5'-CGCAGGGCCGTG**GAG**GAGCTGGACGCCAAG-3'	30
TH-S19E-R	5'-CTTGGCGTCCAGCTC**CTC**CACGGCCCTGCG-3'	30

* Mutated nucleotide are written in bold letters

nt= Nucleotide

4.1.2 Mutagenesis

PCR sample reactions were prepared in accordance with Stratagene® and contain the following:

2.5 µL 10X reaction buffer

0.75 µL Quick solution

1µL (100 ng) plasmid dsDNA template (pcDNA™6.2/nTC-Tag-DEST (Life Technologies)

1 µL (100 ng/µL) Oligonucleotide primer (forward)

1 µL (100 ng/µL) Oligonucleotide primer (reverse)

1 µL (10mM) dNTP mix

17.75 µL ddH_2O

1 µL *Pfu*DNA polymerase (2.5 U/µL)

The PCR program consisted of an initial denaturation at 95º C for 1 minute, followed by 30 1-minute denaturing cycles at 95º C, 1 minute annealing at 55º C and 16 minutes extension at 65º C.

The methylated parental plasmid was digested by adding 1 µL *Dpn*I restriction enzyme (10 U/µL) and incubating it at 37º C for 1 hour. 2 µL of *Dpn* I treated PCR product were transformed into previously thawed ultracompetent XL-10 Gold bacteria (Stratagene®) by 45 minutes ice incubation followed by a brief heat shock of 42º C for 45 seconds before incubating on ice for 2 minutes. SOC medium was added into the bacterial suspension which was incubated at 37º C and 200 rpm for 45 minutes. The transformed cells were then grown at 37º C overnight on LB agar plates with ampicillin (0.1mg/ml) as the selection antibiotic. Several colonies were obtained and two were selected to inoculate LB-medium with ampicillin (0.1mg/ml) for plasmid propagation and purification.

4.1.3 Plasmid purification and sequencing

Plasmidic DNA was purified using QIAprep spin Miniprep kit (QIAGEN) following the manufacturer's protocol. DNA concentration was measured on a NanoDrop instrument (Saveen Werner) and plasmid preparations were routinely diluted to a concentration of 100 ng/µL.

Purified plasmid DNA was prepared for DNA sequencing reaction.

1 µL BigDye®

1 µL sequencing buffer

0.64 µL primer

3 µL (100 ng/µL) plasmid DNA template

4.36 µL ddH_2O

The initial sequencing cycle was set at 96º C for 5 minutes followed by 25 cycles of 96º C for 10 sec, 50º C for 5 sec, 60º C for 4 minutes. DNA sequencing was performed at the Sequencing facility, High Technology Centre, University of Bergen. The mutated sequences were verified by alignment with human TH sequence isoform 1 using the BLAST nucleotide on-line tool (https://blast.ncbi.nlm.nih.gov/Blast.cgi?PAGE_TYPE=BlastSearch).

c.TH1[55T>G;57T>G] (p.TH1S19A) which denotes T to G change at nucleotide 55 and T to G change at nucleotide 57 and c.TH155_57delinsGAG (p.TH1S19E) which denotes the

replacement of nucleotides 55 to 57 by GAG. Nucleotide numbering is in relation to the translation initiation codon of hTH1 (Figure 5.1), starting with number 1 at the A of the ATG. These changes target the serine residue at position 19 to generate phospho-null (S19A) and phospho-mimic (S19E) mutants respectively in the human tyrosine hydroxylase isoform 1 (hTH1) coding sequence that had been previous inserted into a pcDNA 6.2 nTC-tag vector.

4.2 Cell culture and transient transfection

Human SH-SY5Y neuroblastoma (<20 passages) cells or human embryonic kidney 293 (HEK293) cell lines were maintained at 37^0C and 5% CO_2 in Dulbecco's Modified Eagle Medium supplemented with 5% fetal bovine serum (FBS) and 2mM L-glutamine. Cells were grown as a monolayer on P100 plates with 7 ml medium at 37º C in 5% CO_2 and a humidified atmosphere.

At 80-90% confluence cells were detached with 0.25% trypsin for 5 minutes and sub-cultured at a density of 1.2 x 10^6 cells in p60 cell culture dishes for western blot or 2 x 10^4 cells per well in 4-well plates (Nunc) containing laminin:collagen (1.5 mg:1.5mg/ml ratio; Sigma:AdvancedBioMatrix) coated glass cover slips for all imaging experiments. Cells were allowed to grow overnight before being transiently transfected with constructs containing either V5-TH-Wt or V5-TH-S19A or V5-TH-S19E, using Lipofectamine® LTX with PLUS™ reagent (Life Technologies) in accordance with the manufacturer's instructions. The dilution 1 and 2 were mixed before applying to the samples (Table 4.1). When indicated cells were also co-transfected with green fluorescent protein (GFP) using a ratio of 1:3 TH vector:GFP vector.

Table 4.1 Lipofectamine LTX transfection protocol for P60 and 4-well plates.

	P60 plates				
	Dilution1			Dilution2	
	DNA	OptiMEM	PLUS	OptiMEM	LTX
Untransfected control	-	700 µl	10 µl	700 µl	10 µl
V5-TH-Wt	5 µg	700 µl	10 µl	700 µl	10 µl
V5-TH-S19A	5 µg	700 µl	10 µl	700 µl	10 µl
V5-TH-S19E	5 µg	700 µl	10 µl	700 µl	10 µl

	4-well plates					
	Dilution1				Dilution2	
	eGFP	DNA	OptiMEM	PLUS	OptiMEM	LTX
Untransfected control	-	-	50 µl	0.72 µl	50 µl	0.72 µl
V5-TH-Wt	170 ng	500 ng	50 µl	0.72 µl	50 µl	0.72 µl
V5-TH-S19A	170 ng	500 ng	50 µl	0.72 µl	50 µl	0.72 µl
V5-TH-S19E	170 ng	500 ng	50 µl	0.72 µl	50 µl	0.72 µl

Op=OptiMEM reduced media I

Briefly, for p60 plates, 5 µg of V5-TH constructs were mixed with transfecting reagents (Table 4.1) per p60 cell culture dishes, with transfection reagent alone applied to 1 p60 cell culture dish as negative control for western blot analysis. Cells were processed for Western blot after 48 hours post transfection.

For imaging experiments cells were transfected with 0.5 µg per well of V5-TH constructs and when indicated co-transfected with 0.17 µg of green fluorescent protein (GFP) mixed in transfection reagents and applied to 3 wells, with transfection reagent alone applied to the remaining 1 well as a negative control. Cells were grown for 48 hours post transfection in humidified incubator at 37º C in 5% CO_2 before further processing.

4.3 Subcellular fractionation

Transfected SH-SY5Y cells were washed in PBS, trypsinized and collected by centrifugation at 500 g for 10 min at 4º C. The pellets were resuspended in 240 µl of homogenation buffer (5 mMTris-HCl buffer supplemented with protease inhibitor cocktail with EDTA (Roche), Phosphostop (Roche) and 50 mM sucrose). The cells were lysated by passing through a 21G-gauge needle (BD) 20 times. 40 µl of lysate were taken for whole lysate analysis. To the remaining sample sucrose was added to a final concentration of 200 mM. The nuclear fraction was obtained by centrifugation at 900 g for 5 min at 4º C in Beckman Coulter ultra-centrifuge using TLA 120.2 rotor. The nuclei-enriched pellets were resuspended in 40 µl of homogenation buffer supplemented with 1% NP-40. 1% NP-40 was also added to the post-nuclear supernatant and all samples were incubated on ice for 15 min before determining the protein concentration using a Direct Detect spectrometer (Millipore), an infrared based protein quantitation. The nuclear and cytosolic fractions were treated with DNase I RNase free enzyme (Thermo scientific) before preparing them for electrophoretic separation.

4.4 Gel electrophoresis

4.4.1 Blue-Native PAGE

Blue-native PAGE was performed on a continuous-gradient 4-16% NativePAGE pre-casted gel (LifeTechnologies) using light blue cathode buffer (50mM BisTris, 50mM Tricine, 0.1 X cathode additive), anode buffer (50mM BisTris, 50mM Tricine, pH 7.5) and sample buffer following the manufacturer's instructions. 20 µg of nuclear fraction sample and 5 µg of cytosolic fraction sample were treated with DNase I. To 25 µl of each sample, 8 µl of sample buffer 3× and 1 µl of 5% Coomassie G-250 are added. The samples were loaded alongside Native Mark™ protein standard (Invitrogen) and pure humanTH1 and the gel was run in an ice-cold environment. Electrophoresis was started at 150V for 1 hour and increased to 250V for 30 minutes. After electrophoretic separation, the lanes containing native marker and pure humanTH1 were cut, stained with Coomassie 5% and destained in gently agitation with 10% methanol and 10% acetic acid, until a clear background was obtained. The gel with the remaining protein samples were incubated in gentle agitation in transfer buffer (12 mMTris, 96 mM glycine, pH 8.3, 0.1% SDS) for 20 minutes at room temperature before being transferred onto a 0.2 µmpolyvinylidene fluoride (PVDF) membrane using the TurboBlot transfer system from Bio-Rad. Proteins were fixed to the membrane with 8% acetic acid and methanol was used to remove Coomassie stain to avoid interference with the immunoblotting process. Immunodetection was carried out by using the primary antibody mouse anti-V5 (1:5000; Life Technologies) and secondary goat anti-mouse coupled to horse radish peroxidase (1:1000; Life Technologies). Bands were detected using Enhanced chemiluminescence (ECL) system detected by the Chemidoc XRS instrument (Bio-RAD).

4.4.2 Clear-native PAGE

40 µg of nuclear fraction sample and 20 µg of cytosolic fraction sample were mixed with 4× loading buffer (0.2% bromphenol blue; 50% glycerol and loaded in a continuous-gradient 4–16% NativePAGE pre-casted gel (LifeTechnologies) alongside Native Mark™ protein standard (Invitrogen) and pure human TH1. The electrophoretic separation was carried out at 290V for 60 minutes using 50 mMBisTris, 50 mMTricine, pH 7.5 as running buffer in an ice-cold environment. Once the run was completed the lanes containing the native protein standard marker and pure humanTH1 were cut, stained with Coomassie 5% and destained by gentle shaking with 10% methanol, 10% acetic acid, until a clear background was obtained. The remaining protein samples were incubated in transfer buffer (12 mMTris, 96 mM glycine, pH 8.3, 0.1% SDS) for 20 minute at room temperature before being transferred onto

0.2 μm polyvinylidene fluoride (PVDF) membrane using the TurboBlot transfer system from Bio-Rad. Immunodetection was carried out by using the primary antibody mouse anti-V5 (1:5000; Life Technologies) and secondary goat anti-mouse coupled to horse radish peroxidase (1:1000; Life Technologies). Bands were developed using enhanced chemiluminescence (ECL) and detected by a Chemidoc XRS instrument (Bio-RAD).

4.4.3 SDS-PAGE and Immunoblotting

40 μg or 75 μg of the samples were denatured by adding 4× SDS-PAGE loading buffer with a final concentration of 1 mM Dithiothreitol (DTT) and incubation at 95º C for 5 minutes. The samples were centrifuged briefly at room temperature and loaded into pre-casted 10% TGX stain-free gels (Bio-rad) alongside precision plus protein™ dual colour standard (Bio-rad). Electrophoresis was started at 150V for 5 minutes and increased to 180V for 40 minutes. Samples were blotted on to 0.2 μm PVDF membranes using the TurboBlot transfer system (Bio-Rad). The trihalo compound in stainfree gel modifies the tryptophan residues in the protein sequence allowing the fluorescent detection of total protein and facilitating the total protein as a loading control. Immunodetection was carried out by using the primary antibody mouse anti-V5 (1:5000; Life Technologies), rabbit anti-total TH (1:1000; Thermo Scientific) and rabbit anti-THpS19 (1:1000; Phosphosolutions) and secondary goat anti-mouse coupled to horseradish peroxidase (1:1000; Santa Cruz) and goat anti-rabbit coupled with horse radish peroxidise (1:1000; Santa Cruz). Bands were detected using Enhanced chemiluminescence (ECL) system detected by the Chemidoc XRS instrument (Bio-Rad). Band intensity quantification was performed with Imagelab software version 5.1 (Bio-Rad) using the local background settings.

For example for the nuclear fraction of one construct the analysis would be as follows:

$$\frac{\frac{Nuclear\ V5\ intensity}{Nuclear\ total\ protein\ intensity\ lane}}{\frac{Whole\ lysate\ intensity}{Whole\ lysate\ total\ protein\ intensity\ lane}}$$

The values obtained in this way for each mutant construct were referred to the wild type which as arbitrarily taken as 1. T-tests were used in the statistical analysis of western blot studies of distribution of V5-TH constructs.

4.5 Immunofluorescence

Both transfected or non-transfected SH-SY5Y cells were washed with PBS, fixed with 4% paraformaldehyde for 30 min, and permeabilized with 0.2% Triton X-100 in PBS for 5 minutes followed by 5 min washing thrice. Denaturation of fixed cells were carried out by treating the samples with 6M guanidine hydrochloride (GuHCl) before samples were blocked with 5% FBS in PBS. The primary antibodies, mouse anti-V5 (1:200; Life Technologies), mouse anti-total TH (1:100; Santa Cruz), rabbit anti-total TH (1:100; Thermo scientific), rabbit anti-THpS19 (1:50; Phosphosolutions), rabbit anti-pan 14-3-3 (1:100; Abcam), mouse anti-14-3-3 γ (1:100; IBL-America) and secondary antibodies, AlexaFluor 555 goat anti-mouse IgG (H+L; 1:200; Invitrogen), AlexaFluor 488 goat anti-rabbit IgG (H+L; 1:200; Invitrogen), AlexaFluor 647 donkey anti-rabbit IgG (H+L; 1:200; Invitrogen) were used for immunodetection. Samples were mounted with prolong gold mounting media (Thermo Fischer) with DAPI to stain the nucleus. Samples were observed by using Leica confocal microscope TCS SP5 and the images were processed with LAS AF lite software (Leica) as described in the section 4.7.

4.6 Proximity ligation assay (PLA)

Proximity ligation assay was performed using Duolink *In situ* PLA reagents in V5-TH and GFP transiently co-transfected SH-SY5Y cells. The fixation, permeabilization and primary antibody incubation were performed as described in method section 3.13 by using mouse or rabbit anti-V5 (1:100; Life Technologies), rabbit anti-THpS19 (1:50; Phosphosolutions) or rabbit anti-pan 14-3-3 (1:100;). PLA probe dilution/incubation time, rolling circle amplification (RCA) times, polymerase concentrations and wash buffers were prepared in accordance to manufacturer's instructions.

In brief, species specific PLA secondary probes (raised in mouse and rabbit) were diluted at 1:5 ratios in PBS and applied to the samples and incubated at 37 ºC for 60 min. Ligation stock was diluted at 1:5 ratio in deionized water and ligase was diluted at 1:40 ratio. Samples were washed for 5 min twice with buffer A (0.01 M Tris, 0.15 M NaCl and 0.05% Tween 20) before hybridization and ligation was carried out for 30 minutes at 37 ºC. The amplification stock was diluted at 1:5 ratio in deionized water and polymerase mixed with fluorescently labelled oligonucleotides were diluted at 1:80 ratio. Washing of the samples were carried out with wash buffer A for 5 min twice, before amplification was carried out for 100 min at 37

ºC. Samples were washed with buffer B (0.2 M Tris and 0.1 M NaCl) for 10 min and 0.01× buffer B for a min before mounting with ProLong Gold media with DAPI (Thermo Fischer).

4.7 Confocal microscopy

Confocal microscopy images were recorded by a resonant scanner Leica microscope TCS SP5 (Leica Microsystems GmbH, Mannheim, Germany) using a HCX PL APO lambda blue objective with magnification of 63.0x, numerical aperture 1.40 oil immersion UV lens. A pinhole of 1 airy unit (AU) was selected for best signal/noise. Images were 512x512 pixels, a line-average of 4 and a frame-average of 6 were selected. Protein of interest was labelled indirectly with various Alexa Fluor dyes which is conjugated with secondary antibodies and detected by excitation from selected lasers. For example, GFP or pan 14-3-3 labelled with Alexa Fluor 488 were observed by excitation from argon laser at 488 nm, whereas TH labeled with Alexa Fluor 488 or 555 was observed by excitation from argon or DPSS laser at 488 or 555 nm respectively. V5-TH constructs (Wt, S19A and S19E) were labelled with AlexaFluor 555 and observed by excitation from DPSS laser at 561 nm. PLA signals were detected by the excitation from DPSS laser at 555nm. DAPI stain was observed by excitation from blue diode laser at 405 nm. In all cases, the laser power was adjusted to minimize the photo bleaching.

Images were taken when most of the nuclei were in focus. Z-stacks were acquired every 0.21 µm starting at the coverslip surface and ending when the cell monolayer was out of focus. Images were processed with Las AF Lite software (Leica) with minimum adjustment of brightness and contrast.

Single confocal planes corresponding to the region of the cell in which both nucleus and cytosol are focused were chosen for quantification. Signal intensity of the channel of interest was measured using the quantification tool from Las AF Lite software. Briefly, a region of interest (ROI) corresponding to either the nucleus or the cytosol were manually determined and the arithmetical mean intensity was automatically calculated by the Las AF Lite software for each ROI. The values were statistically processed as detailed in the statistical analysis section 4.8.

Tridimensional reconstructions of the images were carried out by Imaris software by Bitplane. Initially, using ImarisColoc, the region of interest (ROI) was masked and the intensity threshold (same for all the images) from the source channels were adjusted to create

the co-localization channel. This allows performing a co-localization analysis of diffused signal. Tridimensional reconstruction of the co-localized ROI was carried out by choosing the isosurface from the object toolbar of Imaris. Similarly, quantification of PLA signals were carried out by creating the co-localization channel of the ROI as mentioned above. The signals in the co-localized channel were detected by spot component of Imaris. The values obtained were statistically processed as detailed in next section.

4.8 Statistical analysis

Western blot bands and confocal microscope images were quantified using Image lab 5.1 beta (described in section 4.4.3), Las AF Lite software or Imaris software (described in section 4.7). The intensities from the different samples (sample size (n) specified in each experiment) were processed using Excel to calculate the average and the corresponding standard deviation (SD). 2-tail paired t-test were used to compare the data sets and statistical significance was set at p-value <0.05. The graphs in this report show the mean intensity value ± SD and the statistical significance when appropriate (* if p-value <0.05; ** if p-value <0.01; *** if p-value <0.001).

5. RESULTS

5.1 Site-directed mutagenesis, plasmid purification and sequencing

In order to generate predicted phospho-null and phospho-mimicking V5-TH versions, we used site-directed mutagenesis and specific primers bearing the nucleotide changes that produced p.TH1-S19A (c.TH1[55T>G;57T>G]) and p.TH1-S19E (c.TH155_57delinsGAG).

The mutated plasmid vectors were subsequently transformed into ultra competent XL-10 Gold bacteria and grown selectively on LB agar containing ampicillin (0.1mg/ml). Four colonies from each mutant were selected and further grown in liquid LB for plasmid purification.

The sequencing of the plasmids showed the incorporation of phospho-null and phospho-mimicking changes at position 19. To visualize the results, we performed a sequence alignment using BLAST nucleotide online tool, comparing the wild-type (Wt) sequence to the mutated ones. Figure 5.1 show that nucleotide thymine is substituted to guanine at position 55 and 57 to produce phospho-null mutant, whereas the phospho-mimicking mutant was produced by substituting two thymines and one cytosine by guanines and adenine from position 55 to 57.

Figure 5.1 Sequence alignment using nucleotide BLAST https://blast.ncbi.nlm.nih.gov/Blast.cgi. The nucleotide alignment shows the incorporation of phospho-null (c.TH1[55T>G;57T>G]) and phospho-mimic (c.TH155_57delinsGAG) changes at position 19.

The nucleotide sequence of Wt, phospho-null and phospho mimic construct were converted to amino acid sequence and aligned with amino acid sequence of human TH using Uniprot online tool to confirm that the base pair changes made during the mutagenesis process were indeed the desired changes at the protein level. Figure 5.2 shows that in Wt (A) a serine is in position 19 which is substituted by alanine or glutamate creating the predicted phospho-null (B) and phospho-mimic (C) mutants, respectively.

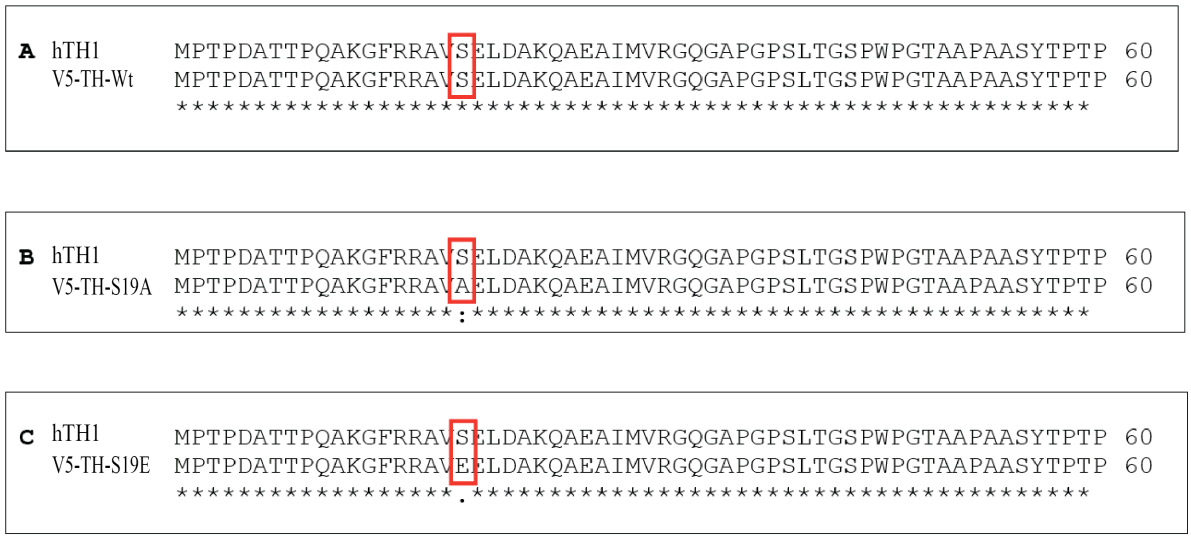

Figure 5.2 Amino acid sequence alignment of hTH1 with A: TH1-Wt, B: TH1-S19A and C: TH1-S19E resulting from the DNA sequencing and translation of mutated plasmid using unirpot online tool (http://www.uniprot.org/).

5.2 Antibody validation

In order to validate the specificity of the anti-V5 and anti-THpSer19 antibodies, we transiently transfected the TH-lacking cell line HEK293 with the V5-TH constructs of interest, namely V5-TH-Wt, V5-TH-S19A and V5-TH-S19E. An untransfected sample was carried in parallel as a negative control. 48 h post-transfection, whole lysates were analysed by Western blot using antibodies against THpSer19 and V5 epitopes. As expected, the lane corresponding to V5-TH-Wt, which can be phosphorylated at all sites, shows a band when detected with THpSer19. However, no band is observed neither for V5-TH-S19A, V5-TH-S19E nor the untransfected samples (Figure 5.3). The additional band of lower molecular weight seen in the V5-TH-Wt lane is most probably due to protein degradation. It is interesting that the antibody did not recognize the V5-TH-S19E construct as a phosphorylated TH at Ser19. Previous data from our lab however indicated that purified non-tagged recombinant TH-S19E did not bind 14-3-3, supporting that the Ser>Glu change does not mimic all the properties of the phosphorylation at Ser19.

In a similar way, the lane corresponding to samples transfected with V5-TH mutants, which has V5 tag at the N-terminal of the fusion protein, showed bands when detected by V5-antibody (Figure 5.3). The V5 signals from the transfected samples are specific as the untransfected control showed no band, as expected.

Thus, our results show that THpSer19 antibody is specific for TH phosphorylated at Ser19, which will occur intracellularly in the Wt protein, and that V5 antibody only recognizes the epitope present in the recombinant protein.

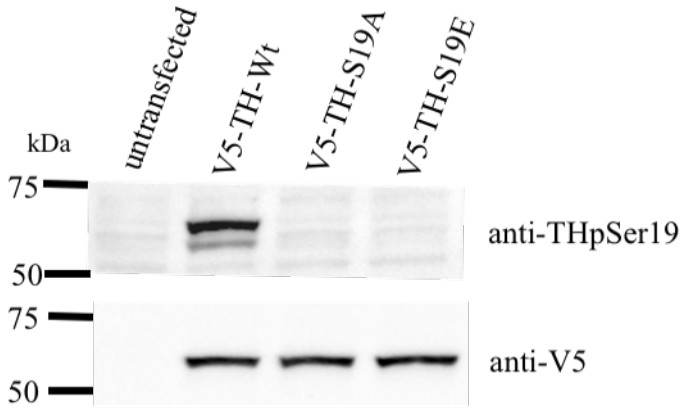

Figure 5.3 SDS-PAGE validations of anti-THpSerine19 and anti-V5 antibodies.

5.3 Oligomeric state of TH in the nucleus

The increased presence of THpSer19 in the nucleus has been reported recently [71] and little is known about the molecular mechanism for this specific subcellular location and/or phosphorylation of the enzyme. Kleppe and collaborators have shown that purified human recombinant TH1 phosphorylated at Ser19 had a higher tendency to become a dimer than the non-phosphorylated TH [14]. Thus, and in order to determine if the nuclear TH is found in a tetrameric form as it is in the cytosol, we investigated its oligomeric state by native-PAGE.

5.3.1 Clear-native PAGE (CN-PAGE)

As it has been reported previously that Coomassie dye may act as anionic detergent and interfere with the native complexes, we choose to begin our studies using clear-native PAGE (CN-PAGE), in which no charged dye is used as opposed to the blue native PAGE method [63].

We first optimized the detergent to be used for the solubilisation and lysis of the nuclear fraction. In particular we treated nuclear fractions of neuroblastoma cells transiently

transfected with V5-TH-Wt with 0.1% Triton X-100, 1% 3-[(3-cholamidopropyl)dimethylammonio]-1-propanesulfonate (CHAPS), 1% NP-40 and 1% digitonin before analysing the samples by CN-PAGE. Since in CN-PAGE protein will separate according to the intrinsic charge of the protein and not to their molecular mass, we included cytosolic fractions and whole lysate of cells transfected with the Wt construct to indicate the position of the tetrameric TH. We also included an untransfected whole lysate sample as a negative control and purified hTH1 as a positive control. The samples were electrophoretically separated and transferred onto PVDF membrane and immunodetected by anti-V5 antibody. The lanes containing the purified TH and molecular weight marker were cut from the gel and stained with Coomasie blue.

Our results show that the nuclear fraction treated with 0.1% triton x-100 showed an inclined band high above 720 kDa, whereas, no V5 signals are detected in the nuclear fraction samples treated with 1% CHAPS and 1% digitonin. However, 1% NP-40 treated nuclear fraction showed a band at ~480 kDa, which is similar to TH in the cytosolic fraction and the whole lysate, which are not treated with detergents. Untransfected negative control shows no band specifying the V5 signals of nuclear, cytosolic fractions and whole lysate. As NP-40 showed results similar to the whole lysate, purified TH and cytosolic fraction, we decided to use this detergent for solubilization (Figure 5.4).

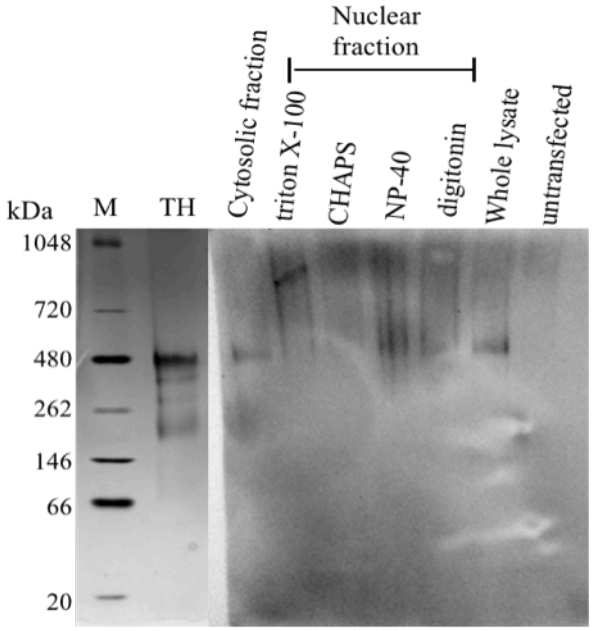

Figure 5.4 Optimization of detergent-based CN-PAGE. The gel was loaded with 0.1% triton X-100, 1% CHAPS, 1% NP-40 and 1% digitonin. Cytosolic fraction and whole lysate were used as positive controls and the untransfected cells as negative control. Immunodetection was carried out by using anti-V5 antibody.

In order to determine the oligomeric state of the TH localized in the nucleus as well as if phosphorylation at Ser19 site had an effect on the oligomeric state we analysed by CN-PAGE the nuclear and cytosolic fractions of neuroblastoma cells expressing V5-TH-Wt, V5-TH-S19A and V5-TH-S19E by CN-PAGE followed by immunoblotting against the V5 epitope of the recombinant proteins. Figure 5.5 shows a single band at the same height in all samples, with no differences between the nuclear and cytosolic fractions or between the different constructs. It was interesting to observe that for all the bands, the apparent molecular mass corresponds to 480 kDa instead of the predicted 240 kDa. However, since these bands are at the same position as purified human tetrameric recombinant TH1, which was run in parallel and its lane was cut out and stained with Comassie G-250 the apparent higher molecular mass is probably due to the limitations of CN-PAGE.

Thus, our data indicate that in these conditions the oligomeric state of TH is the same regardless of localization or phosphorylation at Ser19 site.

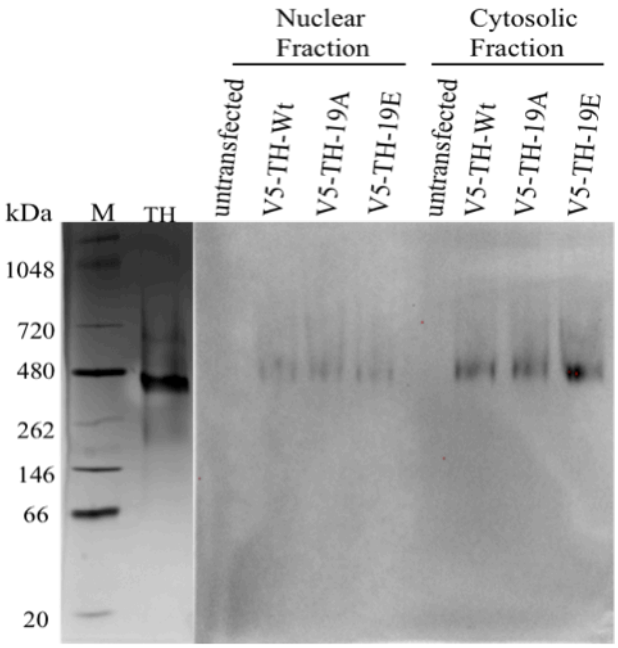

Figure 5.5 CN-Page analysis of native state of TH in nuclear and cytosolic fractions of transiently transfected SH-SY5Y cells. Immunodetection was carried out by using anti V5-TH antibody.

5.3.2 Blue-native PAGE

In order to rule out that size differences were not detected because of the choice of method we decided to also analyse using blue native PAGE (BN-PAGE) the cytosolic and 1% NP-40 treated nuclear fractions of neuroblastoma cells expressing our constructs. As the migration distance in CN-PAGE depends on the protein intrinsic charge, this complicates estimation of oligomerization states and native masses when compared to BN-PAGE, which uses anionic Coomassie-dye to impose a charge shift on the proteins and has higher resolution than CN-PAGE [63].

Our BN_PAGE results show that the molecular weight of all V5-TH variants, both in the cytosolic and nuclear fractions, is ~480 kDa, as seen in CN-PAGE (Figure 5.6). The purified TH showed various sizes ranging from 480 kDa to 60 kDa, the latter corresponding to the apparent Mw of the TH subunit. A dimeric form of about 140 kDa is also detected, similar to the observation by Kleppe, Rosati et al in 2014 [14]. The untransfected controls gave no signal for V5 detection indicating that the signals in the remaining lanes are specific.

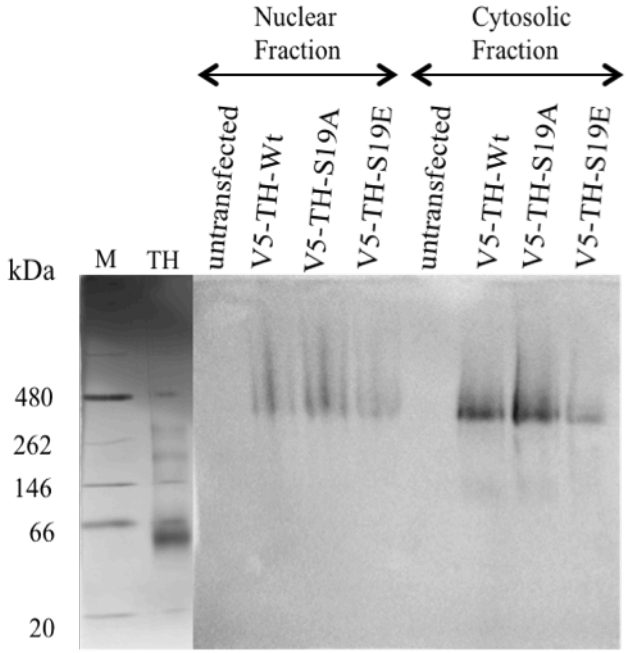

Figure 5.6 Analysis of oligomeric state of V5-TH wt and S19A or S19E variants in nuclear and cytosolic fractions of transiently transfected SH-SY5Y cells. The molecular weight of the standard proteins (M) is given at the left side of the blot. The lane TH represents purified recombinant hTH1 (human TH isoform 1).

Thus, the results from CN-PAGE and BN-PAGE collectively support no dimerization of TH upon phosphorylation at Ser19 and/or nuclear localization.

5.4 Endogenous TH and TH-Ser19 distribution in neuroblastoma cells

In order to study the biological relevance of the phosphorylation of TH at Ser19, we first analysed the cellular distribution of the endogenous proteins in our neuroblastoma cellular model using immunofluorescence and Western blot.

5.4.1 Subcellular distribution of endogenous total TH

The distribution of endogenous TH in neuroblastoma cells was studied by immunofluorescence using rabbit anti-total TH antibody and images were acquired on a TCS SP5 Leica microscope. Our results show that TH protein was distributed throughout the cell (Figure 5.7). The fluorescence intensity measurement was carried out by using LAS software and has been expressed in arbitrary units of intensity (AU). Comparison of the nuclear and cytosolic signal intensity showed that the intensity of total TH was 1.2 times higher in the nucleus than in the cytosol (1036.7 AU ±254.6 in nucleus *vs.* 820.7 AU ±161 in the cytosol; n=13; Figure 5.8).

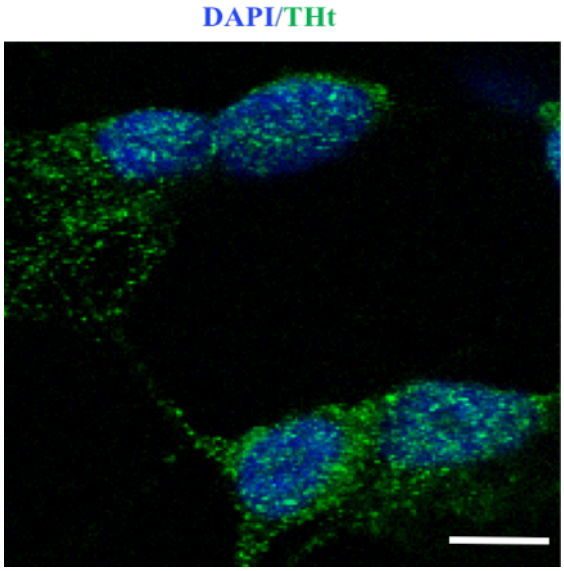

Figure 5.7 Immunofluorescence analysis of endogenous TH. Neuroblastoma cells were immunostained with rabbit anti-total TH antibody. Representative images of confocal plane and orthogonal projection were observed using Leica microscope TCS SP5. Scale bar, 10 µm.

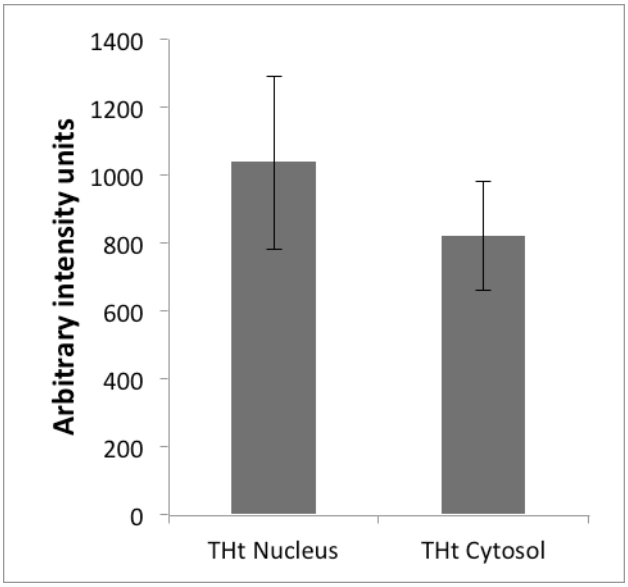

Figure 5.8 Comparison of subcellular distribution of endogenous TH in neuroblastoma cells. TH is 1.2 times higher in the nucleus when compared to cytosol. The fluorescence intensity was measured by LAS software (n=13).

We confirmed our immunofluorescence results using Western blot to detect total TH in nuclear and cytosolic fractions from neuroblastoma cells loading equal amounts of protein from each fraction. Our results show that the band intensity of TH in nuclear and cytosolic fractions are similar (Figure 5.9).

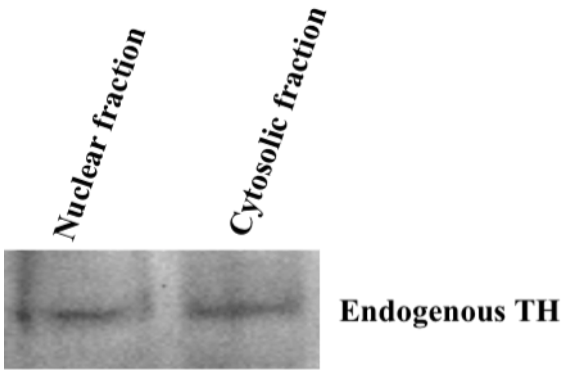

Figure 5.9 Western blot analysis of the distribution of endogenous TH in neuroblastoma cells using anti-total TH antibodies. The band intensity in nuclear and cytosolic fractions are similar.

5.4.2 Sub-cellular distribution of endogenous THpSer19

The distribution of endogenous THpSer19 in neuroblastoma cells was studied by immunofluorescence by using a rabbit anti-THpSer19 antibody and a TCS SP5 Leica microscope to acquire the images. Figure 5.10 shows that THpSer19 is mostly observed in

nucleus, as previously reported by Nakashima et al [71]. Fluorescence intensity analysis illustrated that THpSer19 intensity was 2.2 times higher in nucleus than in the cytosol (2890.8 AU ±280 in the nucleus *vs.* 1313 AU ±164.8 in the cytosol; p-value<0.0001; n=13; Figure 5.11).

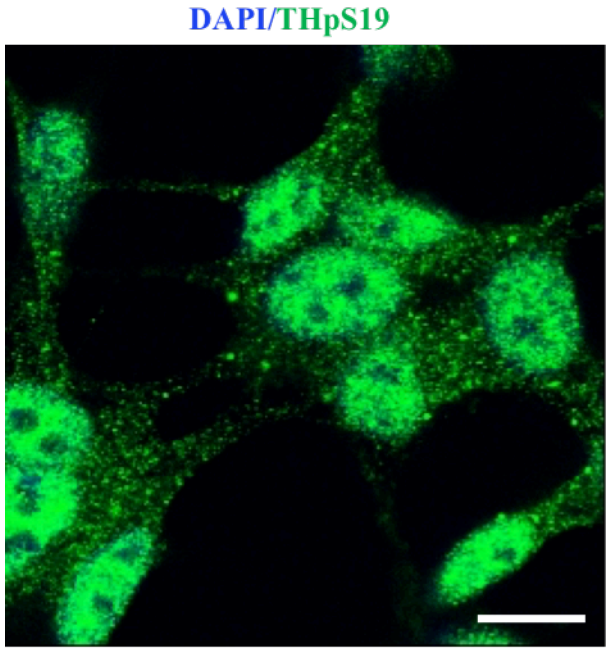

Figure 5.10 Immunohistochemistry of endogenous THpSer19. Neuroblastoma cells were immunostained with rabbit anti-THpSer19 antibody. Representative images of confocal plane and orthogonal projection were observed by using Leica microscope TCS SP5. Scale bar, 10 µm.

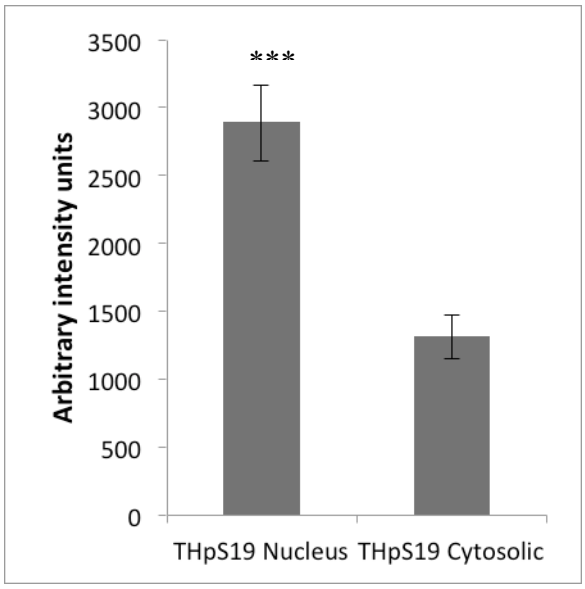

Figure 5.11 Comparison of cellular distribution of endogenous THpSer19 in neuroblastoma cells. THpSer19 is 2.2 times higher in the nucleus when compared to cytosol. The fluorescence intensity was measured by LAS software by choosing region of interest (ROI) (n=13).

In order to further analyse the distribution of endogenous THpSer19, Western blot was performed using samples from nuclear and cytosolic fraction of neuroblastoma cells with 75 µg total protein, and detected by using anti-THpSer19 antibody. Interestingly, we found that THpSer19 shows stronger band intensity in the cytosolic fraction than in the nuclear fraction (Figure 5.12), in agreement with the traditional view of THpSer19 being located in the cytoplasm.

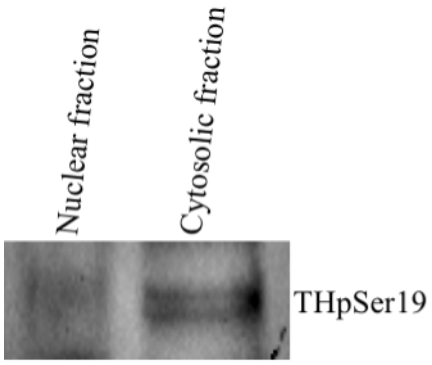

Figure 5.12 Western blot analysis of the distribution of endogenous THpSer19 in neuroblastoma cells by using the rabbit anti-THpSer19 antibody.

We decided to further investigate if the different results obtained by immunofluorescence and Western blotting were related to the methods themselves. Immunofluorescence is a technique that preserves protein:protein interactions whereas Western blot is a denaturing method. In addition, it is well established that THpSer19 binds to the proteins of the 14-3-3 family in a phospho-Ser19 specific manner [72]. Thus, we hypothesized if binding to 14-3-3, and maybe other partners, could be hindering the access of the antibodies to the phosphorylation site in the cytoplasm when performing our *in situ* immunofluorescence assays. Therefore, we detected THpSer19 by immunofluorescence in neuroblastoma samples previously treated with a denaturing agent such as 6M guanidine hydrochloride (GuHCl) (Figure 5.13). Cells treated with the denaturing agent still showed an intense THpSer19 signal in the nucleus however the cytoplasmic signal increased compared with the case in the absence of GuHCl. The intensity measurement carried out by LAS corroborated that the fluorescence intensity of nucleus in both GuHCl treated and untreated sample was similar, 2876.7 AU ±332.4 and 2890.8 AU ±280, respectively (n=13), however, there was 18% increase in the THpSer19 intensity in the cytosol of GuHCl treated sample (1555.6 AU ±360.9 GuHCl treated sample vs 1313 AU±164.8 GuHCl untreated sample; p-value <0.05; n=13; Figure 5.14).

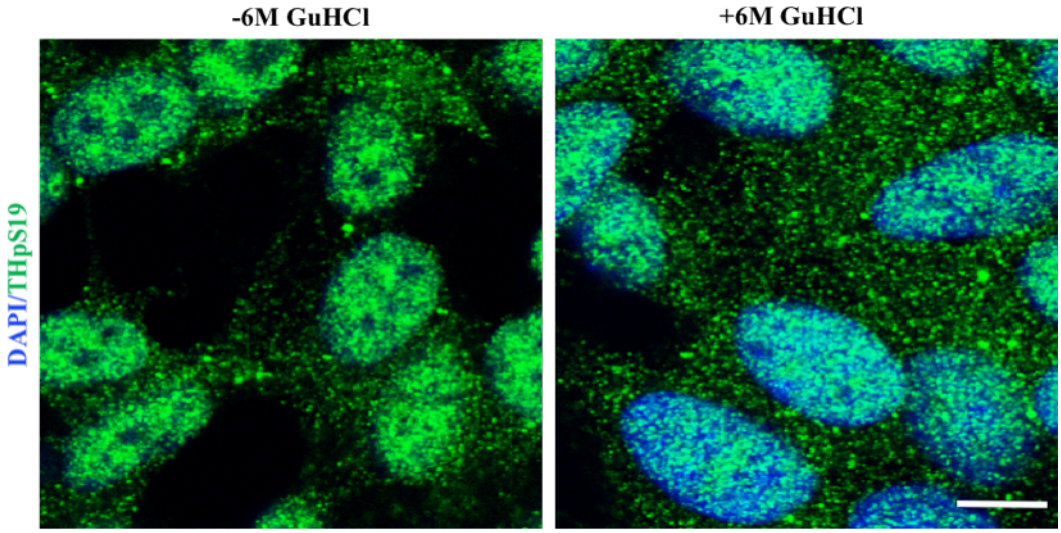

Figure 5.13 Immunofluorescence analysis of the distribution of THpSer19 in neuroblastoma cells treated with 6M guanidine hydrochloride. Representative images obtained using a Leica TCS SP5 microscope. Scale bar, 10 µm.

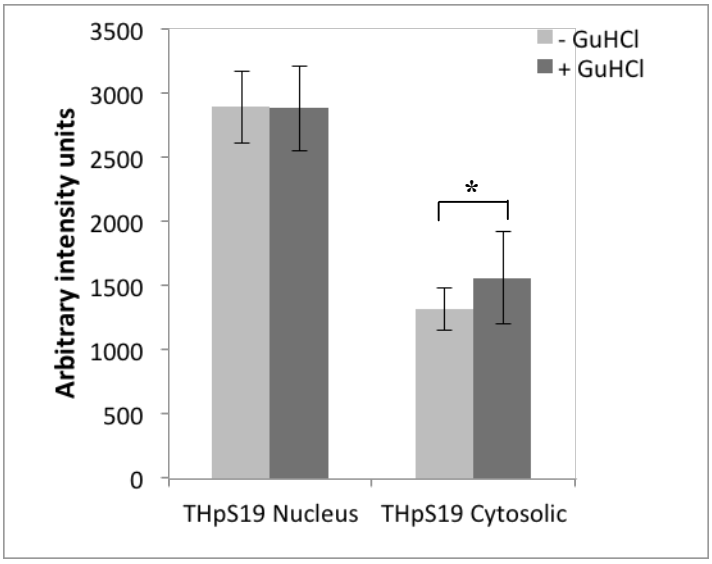

Figure 5.14 Comparison of the distribution of THpSer19 in nucleus and cytosol of neuroblastoma cells treated with GuHCl. The nuclear distribution of THpS19 is similar to the distribution in the absence of GuHCl. The cytosolic intensity of GuHCl treated cells were 18 % higher than in the untreated cells.

5.5 Effect of phosphorylation on the cellular distribution of THpSer19

To study the biological relevance of the specific phosphorylation of TH at Ser19 we used the the V5-TH-Wt, V5-TH-S19A and V5-TH-S19E constructs to analyse potential differences in their cellular distribution.

5.5.1 Effect of phosphorylation on cellular distribution of V5-TH constructs analyzed by immunofluorescence

Before we started investigating the distribution of V5-TH constructs, we validated the behaviour of the Wt construct to ensure that the results that would be obtained with it were comparable to the endogenous TH. We transfected neuroblastoma cells with V5-TH-Wt and performed Western blot followed by detection of TH protein using anti-THpS19 antibody. Figure 5.15 shows higher band intensity in the cytosolic fraction when compared to the nuclear fraction.

Although, only samples of transfected cells with 35 µg total protein were used, the cytosolic fraction shows higher band intensity than the endogenous TH (Figure 5.12), which is due to the high expression levels of the recombinant fusion protein V5-TH-Wt (which has a very similar size as the endogenous TH, 58 kDa *vs.* 55.8 kDa, respectively). The nuclear fraction in Figure 5.15 shows faint band similar to the THpSer19 detected in the endogenous samples (Figure 5.12). Thus, our data indicate that the wild type construct V5-TH-Wt may behave in a similar way as endogenous TH.

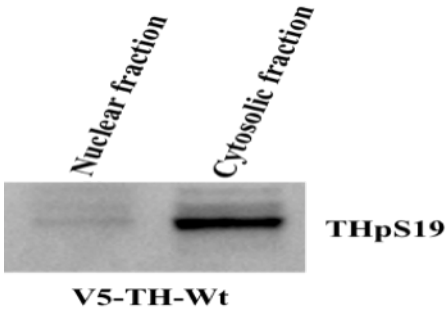

Figure 5.15 Validation of the cellular distribution of the wild-type V5-TH construct by Western blot. THpS19 in nuclear and cytosolic fraction of wild-type V5-TH transfected neuroblastoma cells was detected by using anti-THpS19 antibody.

Following the validation of the Wt construct, we analysed the distribution of the different constructs in neuroblastoma cells. In particular, we transfected SH-SY5Y with V5-TH-Wt,

V5-TH-S19A or V5-TH-S19E and detected the recombinant proteins by immunofluorescence using an antibody against the V5 tag. In parallel, we carried out a negative control using untransfected neuroblastoma cells to show the specificity of the antibodies. Figure 5.16 shows that all V5-TH fusion proteins were predominantly found in the cytoplasm. Nevertheless, this could be due to the characteristics of the constructs in the cytosol, since the vector contains human cytomegalovirus immediate-early (CMV) promoter for high-level expression in a wide range of mammalian cells. We defined the nuclear region using an antibody against the nuclear envelope marker laminin β1. The lack of V5 signal in the negative control (Figure 5.16, top panel) corroborated the specificity of the antibody and ruled out the existence of background staining. Interestingly, certain heterogeneity in the population of Wt construct was observed, with the different degrees of V5 signal inside or around the nucleus. Despite this, both V5-TH-Wt and V5-TH-S19A constructs showed higher nuclear signal intensity than the V5-TH-S19E mutant. The nuclear intensity measurement of each mutant construct was carried out by using LAS software and measured in arbitrary intensity units (AU). The average relative amount of recombinant V5-TH Wt in the nucleus was arbitrarily taken as 100% and was compared with the mutants. Our results, summarized in Figure 5.17, show that, although not statistically significant, the amount of V5-TH-S19A in the nucleus was reduced to 85.7% compared to the wild-type , (470.8 AU ± 234.4 *vs.* 403.5 AU ± 224.7; n=10) whereas, V5-TH-S19E was reduced to 66.5% (470.8 AU ± 234.4 *vs.* 313.2 AU± 158.5; n= 10).

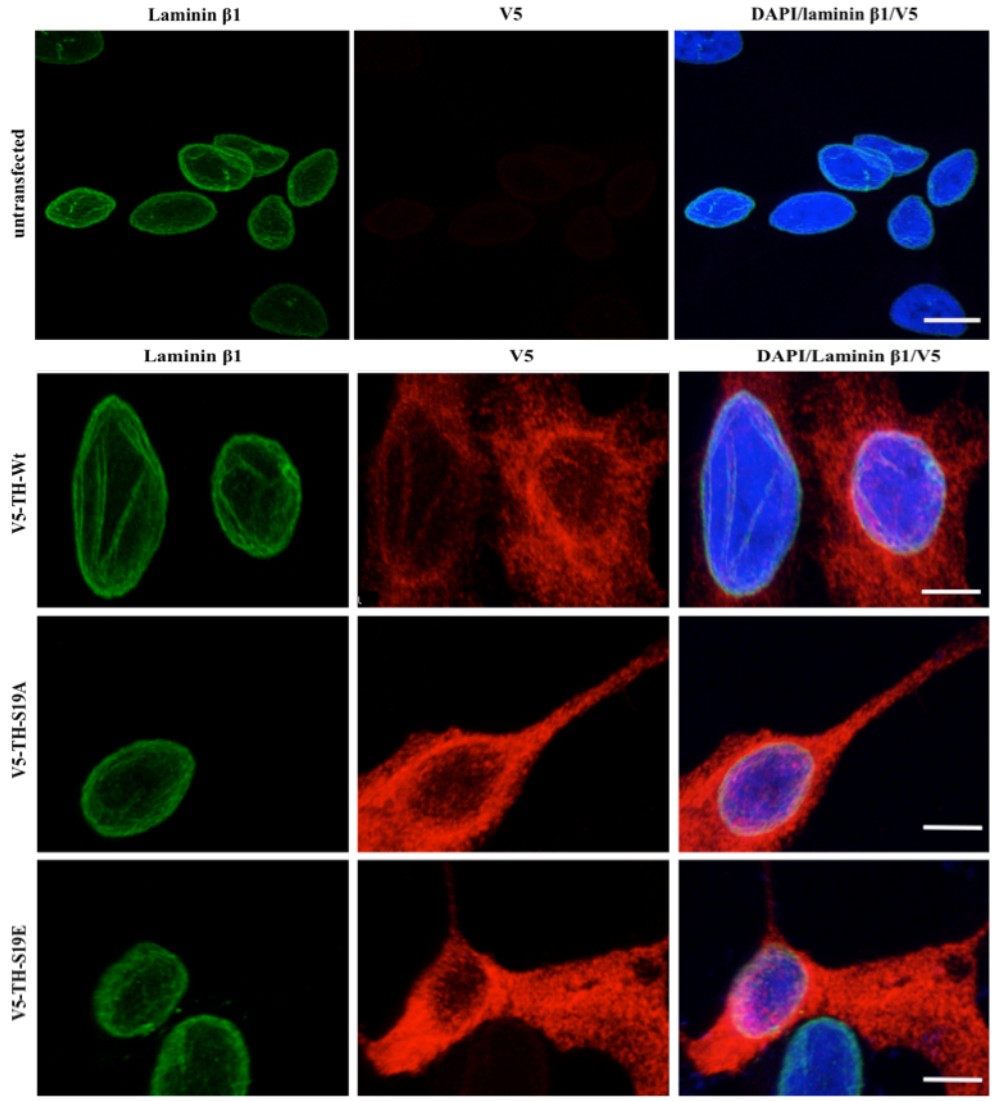

Figure 5.16 Immunohistochemistry of transfected SH-SY5Y cells with V5-TH constructs. Neuroblastoma cells were immunostained with anti-laminin β1 (green), anti-V5 antibody (red channel), and nucleus was stained with DAPI (blue). Top panel shows the negative control. Representative images obtained using a Leica TCS SP5 microscope. Scale bar, 10 μm.

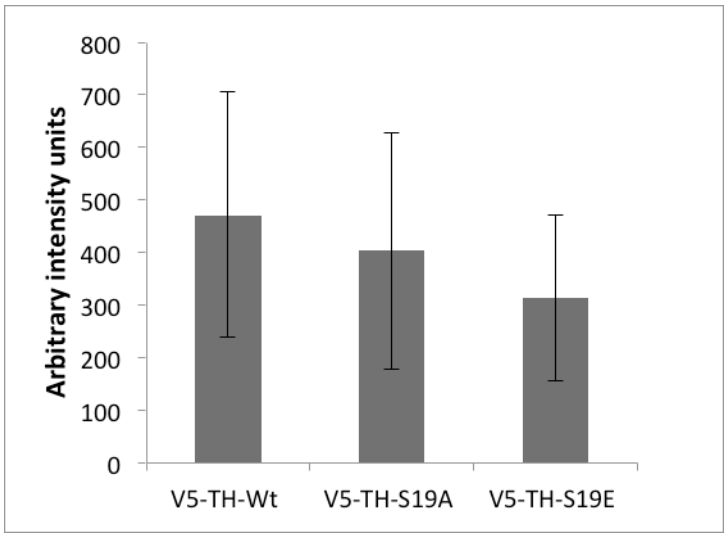

Figure 5.17 Comparison of distribution of V5-TH constructs in the nucleus of neuroblastoma cells. The fluorescence intensity measurement was carried out by LAS software, taking wild type as 1.

However, we observed that the nuclear distribution of V5-TH was different in the cells transfected with the wild-type constructs compared to the mutants. To analyse this with greater detail we carried out a tridimensional reconstruction of the nuclear signal of all the constructs using Imaris software as described in the method section 4.7. The V5 cytosolic signal was represented in white. Nuclear surface rendering was created from laminin β1 staining (green) and the nuclear V5 signal (red). The tridimensional reconstruction shown in Figure 5.18 was performed on the images presented in Figure 5.16. The reconstruction shows that in the case of the wild type construct the distribution of the V5 signal within the nucleus was heterogeneous but could be found occupying most part of the volume. Interestingly, the signal from the mutant constructs seemed limited to the inner surface of the nucleus. However, resolution of the microscope does not allow to determine if the signal is in fact in the inner or outer membrane. In any case, it seems that the mutants show a lower signal and that its distribution is different from that of the wild type construct.

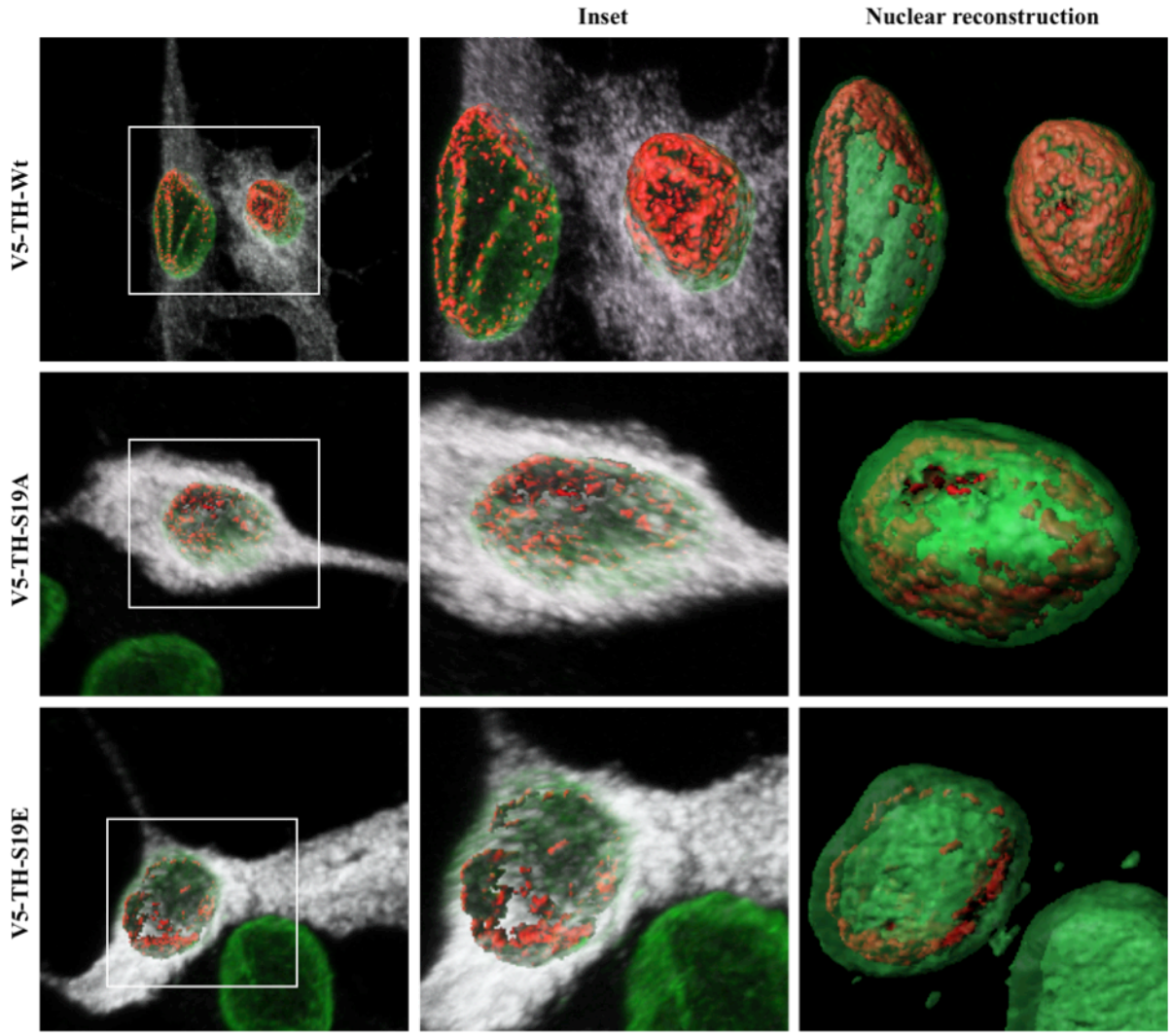

Figure 5.18 3D reconstruction of the nuclear distribution of recombinant TH fusion protein in neuroblastoma cells presented in Figure 5.16. TH fusion protein in the nucleus and cytoplasm is shown in red and white, respectively. The nucleus is reconstructed from the nuclear envelope marker, laminin β1 staining (green). The first column shows the whole cell, whereas the second column shows the enlarged image of the inset. The third column represents only the nuclear V5 and the laminin β1signals.

5.5.2 SDS-PAGE analysis of effect of phosphorylation on cellular distribution of V5-TH constructs

Given that the immunofluorescence results in the previous section 5.4 indicated that the phosphorylation of Ser19 could be playing a role in the nuclear distribution of TH, we decided to investigate this further. In particular we analyzed the cellular distribution of TH using subcellular fractions of SH-SY5Y cells expressing V5-TH-Wt, V5-TH-S19A and V5-TH-S19E followed by immunodetection of the V5 tag (Figure 5.19A). Total protein loading was detected using the stain free detection system (Bio Rad) (Figure 5.19B) and was used as loading control standardization. We observed certain differences regarding the intensity of

the V5 band in the different whole lysates. Thus, to minimize the effect of differences in expression and/or stability levels of the different expressed proteins the nuclear and cytosolic bands of each construct were normalized against the V5 levels present in their corresponding whole lysate.

Figure 5.20 represents the average relative amount of protein present inV5-TH-S19A and V5-TH-S19E samples compared to the Wt (=100%). The relative amount (per total protein) of V5-TH-S19A was significantly decreased to 80% ±12 (p-value <0.05; n=4) whereas V5-TH-S19E was reduced to 65% ±33 (n=4) in the nuclear fraction. In the cytosolic fraction, V5-TH-S19A was comparable to the wild type (103% ±28), whereas, V5-TH-S19E was reduced (66.5% ±47.5) compared to the wild type. V5-TH-S19E data showed high variability in the analysis. Our results indicate that the localization of the V5-TH constructs in the nucleus might not strongly depend on phosphorylation at Ser19.

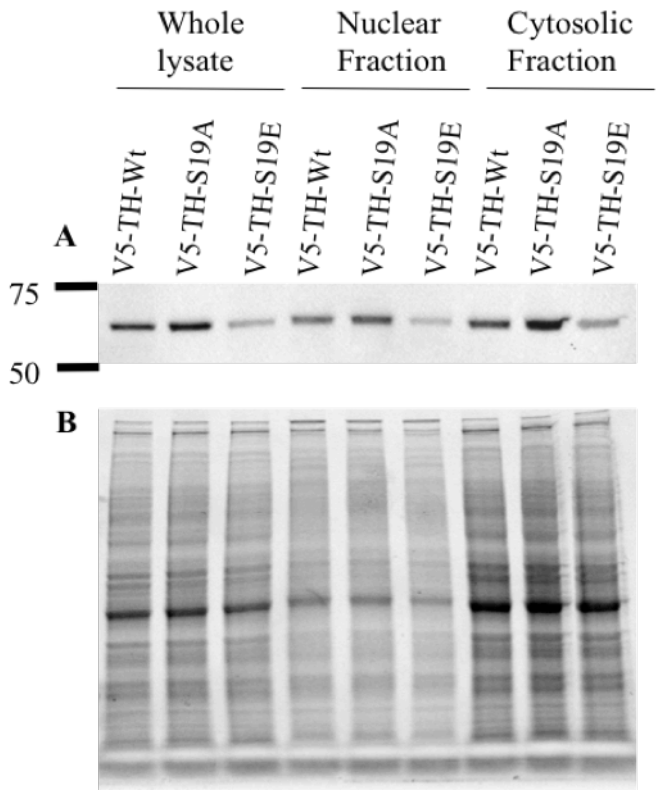

Figure 5.19 Western blot analysis of effect of phosphorylation on cellular distribution of V5-TH constructs in neuroblastoma cells. (A) Immunodetection was carried out by using anti-V5 antibody. (B) Total protein was used as loading control.

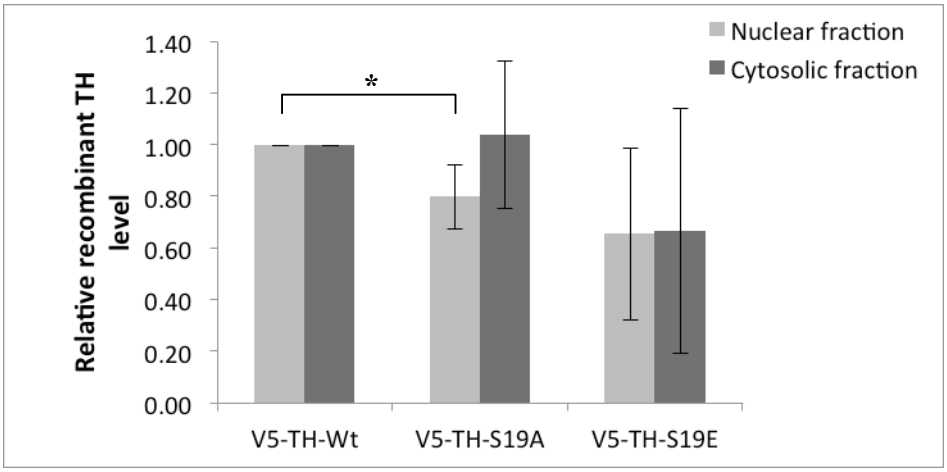

Figure 5.20 Quantification of the V5-tag signal in nuclear and cytosolic fractions. Cellular fractions of neuroblastoma cells expressing V5-TH wild type, S19A or S19E constructs were analysed by Western blot. Compared to the wild type V5-TH-S19A shows a decrease in nuclear fraction and V5-TH-S19E was reduced in both nuclear and cytosolic fraction.

5.5.3 Analysis of distribution of TH and V5-TH constructs using proximity ligation assay (PLA)

We continued our studies by investigating the interaction of TH with its known binding partner 14-3-3 when phosphorylated at Ser19 and analyzed the distribution of V5-TH constructs in neuroblastoma cells using *in situ* PLA.

We first optimized the system to ensure no cross-reactivity of the antibodies since PLA involves an initial detection of the target protein by simultaneous incubation of two primary antibodies raised in different species, similar to immunofluorescence.

SH-SY5Y cells were transiently transfected with V5-TH constructs (Wt and S19A) and co-transfected with GFP as a positive transfection control. V5-TH-S19E was excluded from this part of the study due to the high variability observed earlier in this study (Figure 5.19). Cells were immunostained with mouse anti-V5 (cyan) and rabbit anti-THpS19 (Red).

Figure 5.21 shows that, although the V5-TH constructs are predominantly expressed in the cytoplasm, the nuclear intensity in the case of Wt is higher compared to the V5-TH-S19A mutant, despite of having both cases similar expression level of the constructs (cytosolic V5 signal intensity is comparable), similar to the data from previous immunofluorescence (5.5.1). THpSer19 is primarily localized in the nucleus in both cases, however the nuclear intensity in case of Wt transfected cells is higher than for the phospho-null transfection, which could be the contribution from the recombinant Wt TH that is localized in the nucleus.

Thus, our data indicates that co-transfection with GFP does not alter the distribution of both recombinant and endogenous TH in neuroblastoma cells. Moreover, there seems to be no cross-reactivity of the antibodies used, which was further confirmed by a series of sequential and simultaneous staining (data not shown).

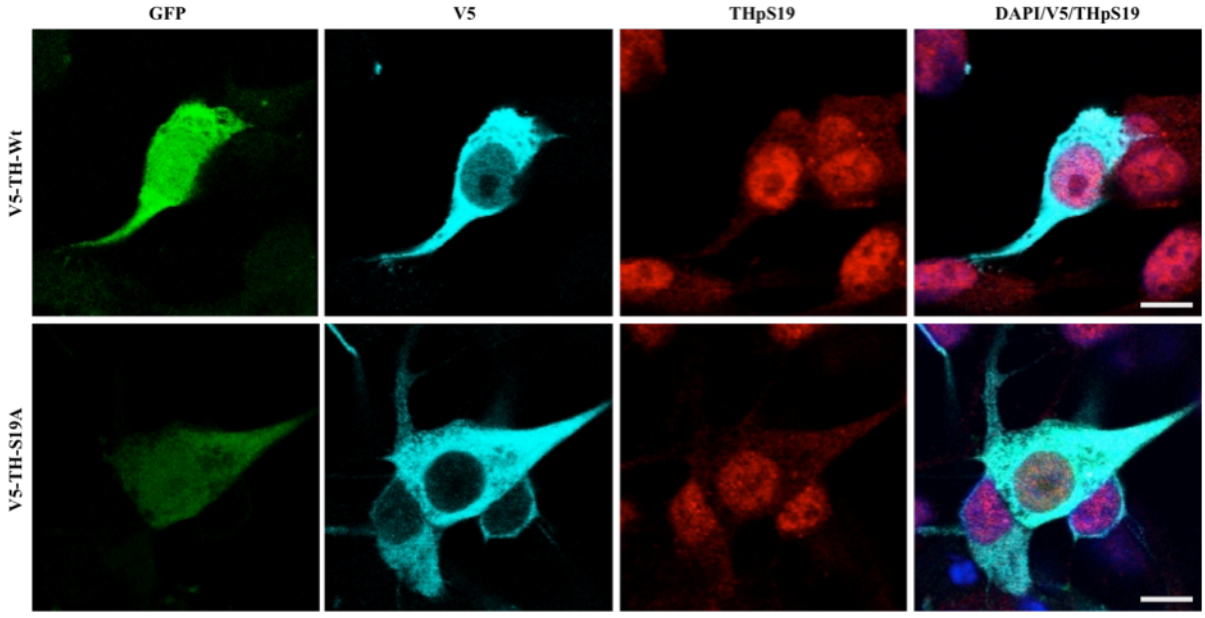

Figure 5.21 Distribution of THpS19 and V5-TH (Wt & S19A) constructs in transfected neuroblastoma cells, co-transfected with GFP (green channel). SH-SY5Y cells immunostained with anti-V5 (cyan) and anti-THpS19 (red) antibodies. Nucleus was stained with DAPI (blue). Images were visualized by Leica Confocal Microscope TCS SP5. Scale bar, 10 µm.

5.5.4 PLA analysis of effect of phosphorylation on cellular distribution of V5-TH constructs

Given the high variability of the nuclear signal in the different constructs, especially for the V5-THS19E construct, we decided to use proximity ligation assays (PLA) to further analyse the cellular distribution of the constructs in our samples.

In order to determine if the TH present in the nucleus is mainly phosphorylated at Ser19 we performed PLA between antibodies against V5 and total TH or THpS19 in neuroblastoma cells expressing V5-TH-Wt and co-transfected with GFP as a transfection marker. In parallel, we carried out a negative control to show that the PLA signal is not an artefact or a background noise.

Figure 5.22 A shows that the cell transfected with GFP in the negative control does not show any PLA signals (red dots), indicating that the results obtained would be specific PLA

signals. Figure 5.22B and C shows PLA signals predominantly distributed in the cytoplasm, indicating that TH is a cytosolic protein as traditionally accepted but that it is also distributed in the nucleus.

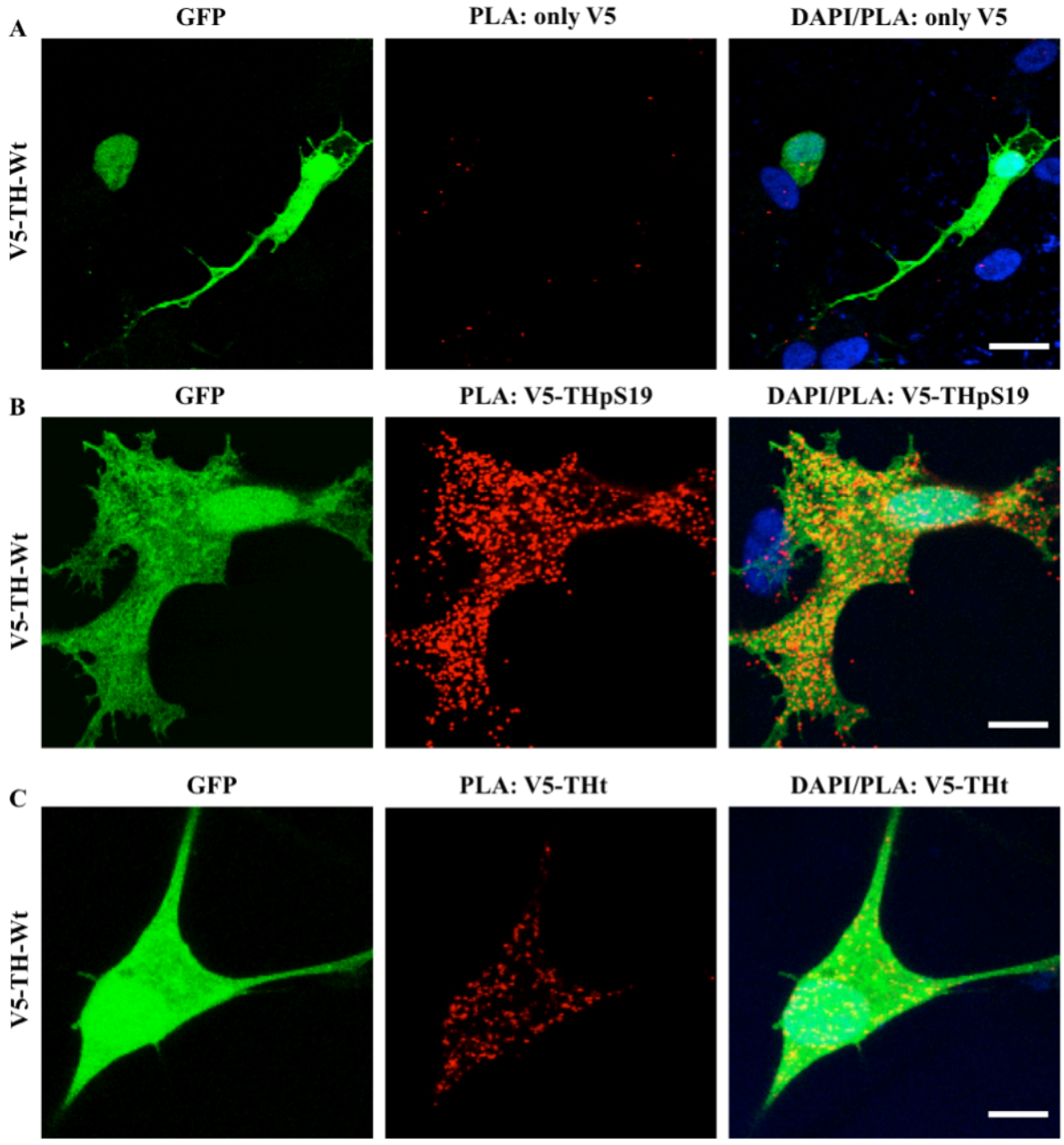

Figure 5.22 PLA analysis of distribution of recombinant Wt-TH in transfected neuroblastoma cells, co-transfected with GFP. Mouse anti-V5 and rabbit anti-THpS19 (B) or rabbit anti-total TH (THt) (C) was used as primary detection to recognize recombinant TH. Species specific PLA probes were used to label the primary detection and were visualized by using confocal microscopy. The nuclei were stained by using DAPI. (A) negative control of the experiment. Scale bar, 10 µm.

The data analysis has consisted, briefly, in quantifying the PLA signals by using the Imaris software (discussed in section 4.7) to determine the average relative amount of Wt-TH distributed in the nucleus and dividing by the whole PLA signal in a cell.

Figure 5.23 shows that approximately 25% of the recombinant Wt-TH is distributed in the nucleus regardless of total TH or THpS19 detection, 24.1% ±4, 25.7% ±11, respectively. Our data support that there are no significant differences in total TH and THpS19 detection and thus, that the TH present in the nucleus seems to be phosphorylated at Ser19.

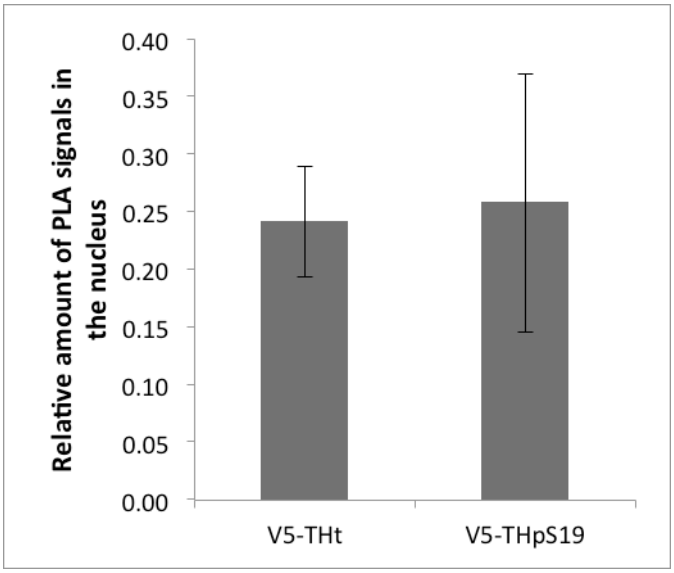

Figure 5.23 Quantification the nuclear PLA signals from V5 and total TH (THt in the graph) or V5 and THpSer19 antibodies in neuroblastoma cells expressing V5-TH wild type.

To corroborate the results obtained in sections 5.51 and 5.52, we performed *in situ* PLA using V5 and total TH antibodies in neuroblastoma cells expressing V5-TH-Wt, V5-TH-S19A or V5-TH-S19E and co-transfected with GFP as a transfection marker. Figure 5.24 shows that TH is predominantly distributed in the cytoplasm and very few PLA signals in the nucleus.

We first calculated the relative amount of PLA signals in the nucleus and cytosol for each GFP-positive cell and obtained an average ±SD for each construct. Wild-type construct showed 24% ±4 of the signal in the nucleus and the remaining 75.9% ±4. Whereas the mutant V5-TH-S19A and V5-TH-S19E showed 20.1% ±8 and 16.1% ±6 in the nucleus and 79.9% ±8 and 82.9% ±6 in the cytosol (Figure 5.25). Thus our data indicated that the amount of PLA signals found in the nucleus is slightly lower for the V5-TH-S19A and V5-TH-S19E mutants (83% and 66% respectively) with a concomitant increase in the cytosol.

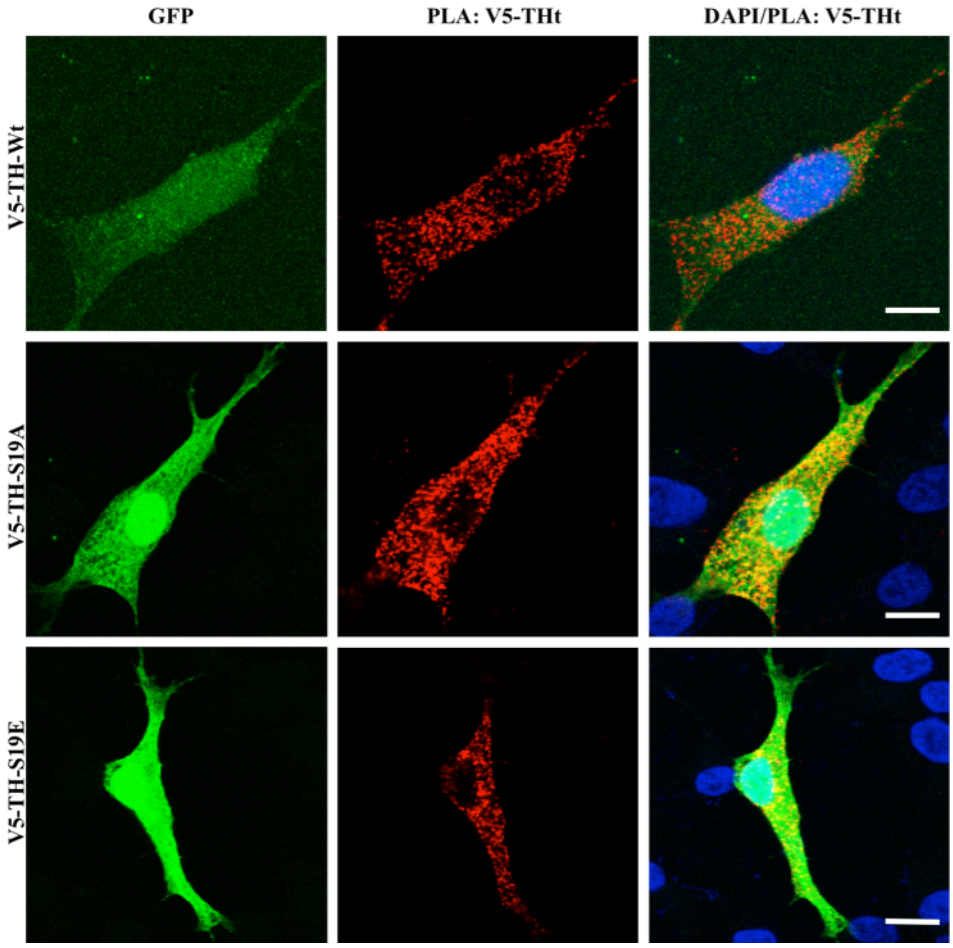

Figure 5.24 analysis of distribution of wildtype, phospho-null and phospho-mimic constructs in neuroblastoma cells. PLA detection of recombinant TH was carried out by using mouse anti-V5 and rabbit anti-total TH as primary antibodies and labelled with species specific PLA probes (red). Nucleus was stained with DAPI (blue). The representative images were observed by using confocal microscope. Scale bar, 10 µm.

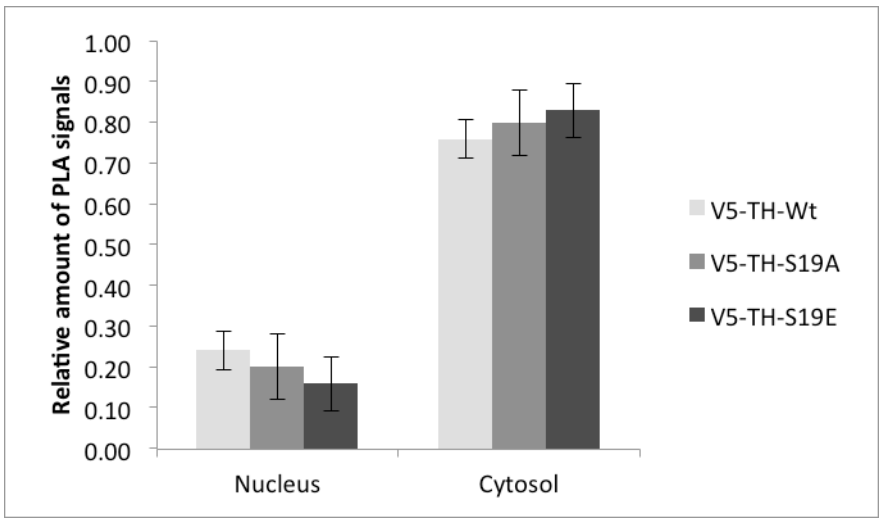

5.25 Comparison of distribution of recombinant V5-TH protein in neuroblastoma cells using in situ PLA. The average percentage of PLA signal in the nucleus and in the cytosol was calculated for each construct and represented in the graph.

The data obtained from the PLA analysis is similar to the data from the Western blot (Figure 5.20). Thus, our data indicate that nuclear localization of TH appears not to be strongly dependent on phosphorylation at Ser19.

We also carried out tridimensional reconstruction of the PLA signals by using Imaris software to show the distribution of V5-TH constructs in the neuroblastoma cells. The cytosolic PLA signal was represented in white. Nuclear surface rendering was created from DAPI staining (blue) and the nuclear PLA signal was also a 3D reconstruction (red). In this case we did not use laminin β1 staining to delimit the nuclear envelope since conventional immunofluorescence is not generally recommended to be combined with PLA assays. The tridimensional reconstruction represents V5-TH constructs from figure 5.24. Figure 5.26 shows that the PLA signals in Wt and V5-TH-S19 constructs are distributed inside and around the nucleus, however, in V5-TH-S19E it is distributed around the inner surface of the nucleus, similar to what we observed in immunofluorescence.

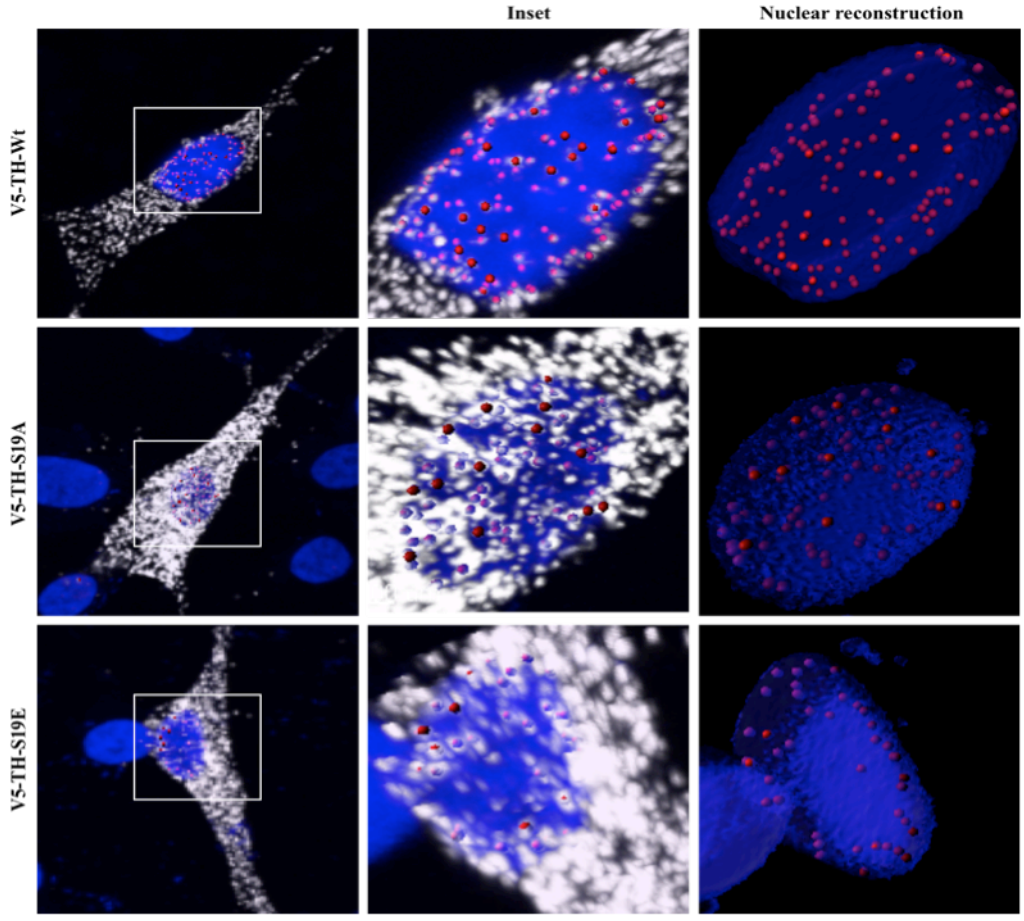

Figure 5.26 of distribution of PLA signals in neuroblastoma cells. TH fusion protein in nucleus and cytoplasm is shown in red and white, respectively. Nuclei are constructed from the DAPI staining (blue). The first column shows the whole cell, whereas the second column shows an enlarged image of first columns inset. The third column represents the nuclear reconstruction of the inset image.

5.6 Interaction of THpSer19 and 14-3-3 proteins in neuroblastoma nucleus

Given that 14-3-3 proteins bind TH when it is phosphorylated at Ser19, and that our results show that the TH found in the nucleus is phosphorylated at Ser19, we decided to investigate if 14-3-3 proteins were also TH partners in the nucleus. Therefore, we began analyzing by immunofluorescence the neuroblastoma distribution of endogenous total TH and 14-3-3, regardless of phosphorylation and isoform respectively.

Figure 5.27A shows that both proteins are present in the nucleus, indicating that THpSer19 could also be interacting with 14-3-3 (pan 14-3-3 in the figure) in this organelle. However, the weakness of the signals suggested that the epitope of the proteins could be masked by partner proteins. Therefore, we also treated the samples with guanidine hydrochloride to denature the proteins and expose the epitopes to the antibodies. Figure 5.27B shows that the intensity of the signals was higher for 14-3-3, and to a lesser extent also total TH, than in the non-treated samples indicating that both TH and 14-3-3 proteins are interacting with partners.

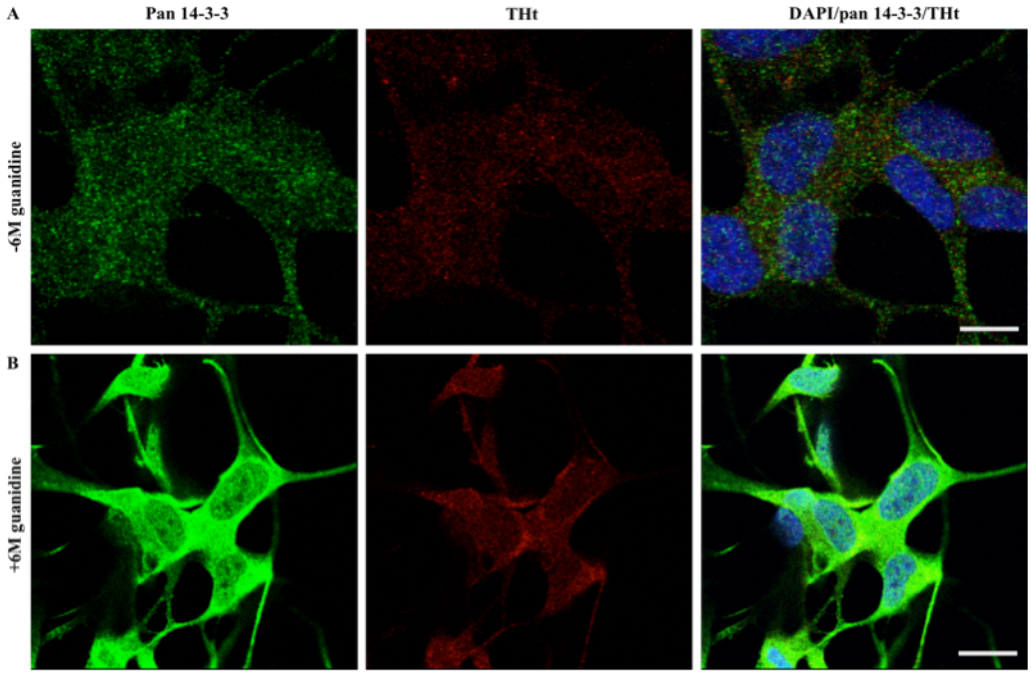

Figure 5.27 Cellular distribution of TH in relation to 14-3-3 in neuroblastoma cells. SH-SY5Y cells immunostained with anti-pan 14-3-3 antibody (green) and anti-total TH antibody (red). (B) SH-SY5Y cells treated with 6M GuHCl. Nucleus stained with DAPI (blue). Images were visualized by Leica Confocal Microscope TCS SP5 under exact same acquisition conditions. Scale bar, 10 µm.

We then continued analyzing the interaction of THpSer19 with 14-3-3, regardless of isoform, using our V5-TH constructs and focusing on the nuclear region of the cells using *in situ* PLA.

Figure 5.28 shows positive PLA signal when using V5 and pan 14-3-3 antibodies in neuroblastoma cells expressing V5-TH wt (upper panels) or the absence of signal when cells express the V5-TH-S19A, used as a negative control of the interaction and highlighting the importance of serine 19 phosphorylation for TH to interact with 14-3-3 proteins described previously for the TH:14-3-3 interaction [73]and by our lab. In both cases GFP was co-transfected and was used as a positive transfection control.

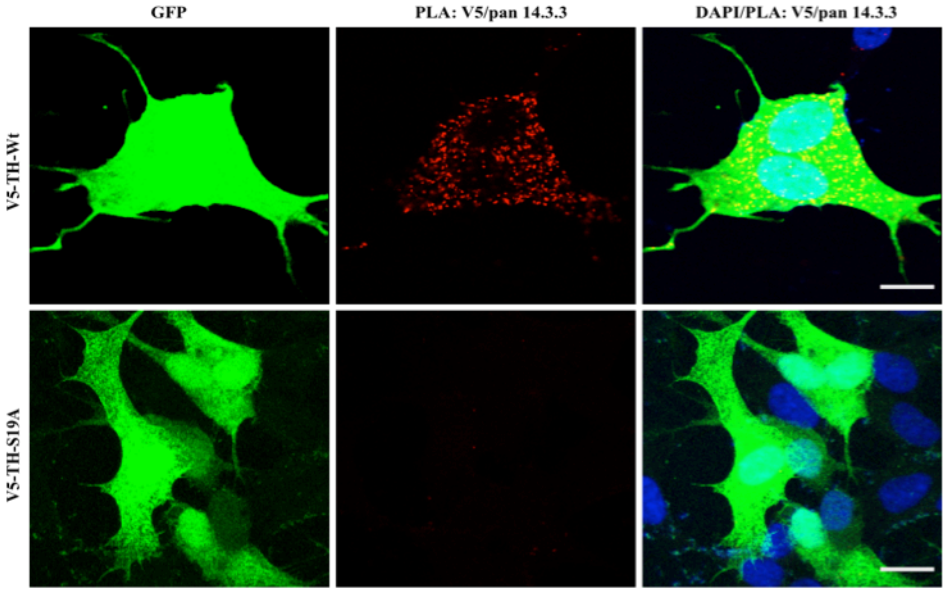

Figure 5.28 PLA analysis of the co-distribution of THpSer19 and 14-3-3 regardless of isoform (pan 14-3-3 in the figure) in neuroblastoma cells. Neuroblastoma cells co-expressing GFP (transfection control) and the wild type or phospho-null mutant. PLA signal was generated by targeting mouse anti-V5 and rabbit anti-pan 14-3-3 primary antibodies by PLA probes. Nucleus was stained by DAPI. Images were observes using confocal microscope. Scale bar, 10 µm.

We quantified the data obtained from the V5/pan 14-3-3 PLA signal by Imaris software, to analyze the relative amount of 14-3-3 proteins interacting with THpSer19 in the nucleus. Figure 5.29 shows approximately 24% ±7 of the total THpSer19/14-3-3 proteins distributed in the nucleus of neuroblastoma cells. Comparing the data from the V5/THpSer19 PLA (25.7% ±11) in section 5.5.4 and the V5/pan 14-3-3 PLA obtained here we do not observe significant differences (Figure 5.29). Thus, our data suggests that THpS19 in the nucleus might be interacting with 14-3-3 proteins.

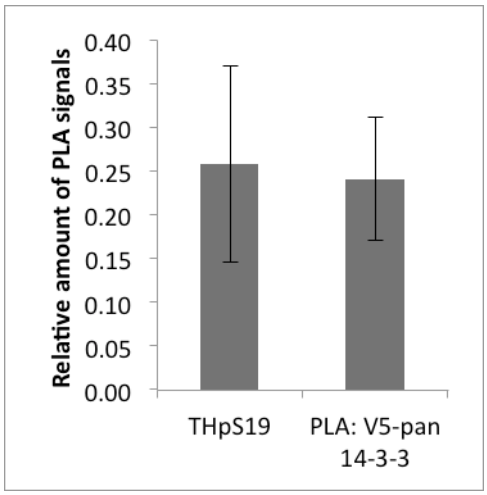

Figure 5.29 Comparison of distribution of THpS19 and THpS19/14-3-3 in the nucleus of neuroblastoma cells using PLA shows no significant differences.

In order to gain further insights into the interaction between THpSer19 and 14-3-3 we began to systematically analyze the co-distribution of THpSer19 with each different isoform of 14-3-3. We first performed a PLA assay using mouse anti-V5 and rabbit anti-14-3-3 γ in neuroblastoma cells expressing V5-Th Wt and GFP as our transfection control. Figure 5.30 shows that THpSer19:14-3-3 γ interaction is predominantly distributed in the cytoplasm. PLA signals were quantified to analyze the average relative amount of 14-3-3 γ in the nucleus, which is approximately 15% ±7.5 of the total PLA signals.

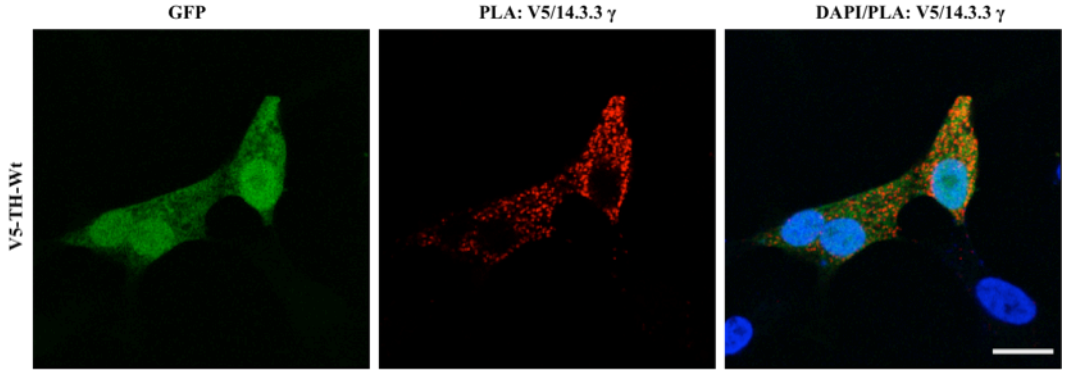

Figure 5.30 PLA analysis of co-distribution of THpSer19 and 14-3-3 γ in neuroblastoma cells transiently transfected with wild type mutant and co-transfected with GFP. PLA signal was generated by targeting mouse anti-V5 and rabbit anti-14-3-3 γ primary antibodies by PLA probes. Nucleus stained by DAPI. Representative images were observed by confocal microscope. Scale bar, 10 μm.

6. DISCUSSION

Phosphorylation is one of the most prominent PTM, generating phosphoamino acids and diversifying the chemical nature of a protein surface [74]. It acts as a key aspect of short-term regulatory mechanisms of proteins in the cell. The addition of a phosphoryl group (PO_3^{2-}) to a protein could exhibit many functions, such as a subtle change in protein structure to modify the active site without changing the overall shape of the molecule, e.g. MAPK activation by phosphorylation [75]. For other proteins such as PAH it has been predicted that phosphorylation causes a larger conformational change, in that case activates the enzyme [76]. In other cases the covalently attached phosphate group imparts a unique size and charge properties aiding inducible protein-protein interaction by allowing phosphoprotein recognition by phosphospecific-binding domains in the protein partner, as is the case for the pSer19-dependent interaction of TH with 14-3-3 proteins [14, 53]. Moreover, it has recently been shown that phosphorylation at Ser19 in TH also leads to increased degradation by ubiquitin-proteasome pathway [71, 77].

The role of phosphorylation of TH has been investigated previously. Phosphorylation at different sites on TH is catalysed by specific kinases. Ser40 is phosphorylated by PKA, protein kinase C (PKC), protein kinase G (PKG), MAPKAPK 1 and 2, CaMPK II, PRAK, mitogen and stress-activated protein kinase (MSK) 1 [27, 33, 35, 36, 78, 79]. Directly or indirectly all these kinases act on Ser40 which leads to increased TH activity by inhibiting the feedback mechanism by catecholamines. Ser31 on the other hand is known to be phosphorylated by only ERK 1 and 2 [29], which also increases the enzyme activity *in vitro* but to lesser extent than Ser40 phosphorylation [26]. CaMPK II was found to be the major kinase responsible to phosphorylate TH at Ser19 [33], whereas MAPKAPK2 [35] and PRAK [36] were found to phosphorylate TH at Ser19 *in vitro*. It is known that Ser19 phosphorylation increased the TH activity when bound to 14-3-3 proteins [56]. However, the recent finding of pSer19 in the nucleus of PC12 cells [71] was found interesting and we therefore addressed the molecular basis of this subcellular localization as well as a possible biological relevance in this study.

6.1 TH mutants

A most prominent technique to unlock the function of phosphorylation is to modify proteins by using a widely accepted tool, such as phospho-site mutations. In order to study the biological effect of absent and complete phosphorylation it is customary to create null and

mimic phosphorylation mutants, respectively. In general, the null mutant corresponds to that with the phospho-site mutated to alanine. A phospho-site substitution to a small hydrophobic alanine is not a critical change and it usually does not influence the microenvironment sufficiently to change the conformation. As null mutation does not interfere with kinase recognition or binding, Szmigielski et al. in 1977 first introduced the concept of null mutation that came from the sequence of regulatory subunit of PKA [80]. The auto-inhibitory domain of the regulatory subunit, which is also known as PKA recognition motif (-Arg-Arg-x-(Ser or Thr)-y-), was maintained with the exception that the Ser/Thr is substituted with Ala, which cannot be phosphorylated [80]. The auto-inhibitory domain promotes PKA binding strongly until the regulatory subunit changes conformation and dissociates. A crystallographer, Hurley JH in 1990 first introduced the concept of phospho-mimic mutation, who wanted to record the phosphorylated structure of an enzyme [81]. A negative charged amino acid, such as glutamic acid or aspartic acid could be used to substitute the phospho-site, rendering the biochemical environment that could mimic phosphorylation in most cases. These mutational approaches allow researchers to anticipate complete phospho-null and phospho-mimic at the desired phospho-sites. However, it should be considered that the phospho-mimic substitutions may fail to reproduce all aspects associated with phosphorylation of a protein, such as the interaction of pSer-TH with 14-3-3 proteins ([73] and data from our lab).

The purpose of this Master thesis has been to investigate the cellular role of Ser19 phosphorylation in TH. In order to study the role of phosphorylation for this project, we implemented the phospho-site mutational technique by substituting Ser residue with Ala or Glu at position 19 of recombinant TH to create phospho-null (V5-TH-S19A) and phospho-mimic mutant (V5-TH-S19E), respectively.

6.2 Oligomeric state of TH

Using the purified recombinant TH (isoform 1 of the human enzyme, hTH1), numerous *in vitro* studies have demonstrated the phosphorylation dependent regulation of TH activity [82], and changes in the phosphorylation of TH *in vivo* have been associated with changes in the activity of TH [83]. We started the project by creating the above mentioned recombinant-TH constructs variants for expression in eukaryote cells using site-directed mutagenesis (Figure 5.1 and 5.2), and used neuroblastoma cells as a dopaminergic neuron model to show the role of phosphorylation in the cellular distribution and oligomeric state of TH.

Taking the recent finding of TH in the nucleus into consideration [71], we hypothesized that a possible functional role of nuclear TH might be related to transcriptional regulation. Indeed, it has been previously shown that pterin-4a-carbinolamine dehydratase (PCD), a tetrameric cytoplasmic enzyme involved in the regeneration of the reduced cofactor BH4 following the TH-reaction (Figure 1.4) plays a dual function and also has a nuclear function as a dimerization cofactor of the transcription factor hepatocyte nuclear factor 1 (HNF1) [84]. For this nuclear cofactor function PCD does not maintain its tetrameric structure but actually dimerizes and binds to HNF1 as dimer. We therefore investigated the effect of phosphorylation on the oligomeric state of recombinant TH in subcellular fractions (nuclear and cytosolic) of neuroblastoma cells using native-PAGE, and immunodetected by using antibody against V5 epitope. It is clear from our data that there is no significant difference in the oligomeric state of TH in the subcellular fractions despite different phosphorylation state of Ser19 (Figure 5.5 and 5.6). It is unclear why TH, that shows a correct size for a tetrameric enzyme by both size exclusion chromatography and dynamic light scattering (Bezem et al., in revision), shows a size by native MS (480 kDa) that rather indicates an octameric configuration (Figure 5.5 and 5.6), pointing to formation of intermolecular interactions, probably by intermolecular disulphide bridges. Moreover, purified TH showed various sizes ranging from 480 kDa to 60 kDa (Figure 5.6). A dimeric form of 140 kDa was also observed, similar to the observation of Kleppe et al [14].

It is known from previous studies that TH tetramer is structurally organized as a dimer of dimers, according to the amino acid sequence alignment data, there are three potential leucine zipper (LZ) motifs (LZ-A, LZ-B and LZ-C) in the catalytic domain of both TH, as demonstrated in the crystal structure of the catalytic and tetramerization domains (Figure 1.6) [85]. In the tetrameric structure each C-terminal α-helix interacts with two other α-helix forming a helix bundle to favour tetramerization [86]. Kleppe et al. have shown that purified THpS19 showed both tetrameric (major) and dimeric (minor) forms, especially when incubated with 14-3-3γ [14]. Also, Xi He et al. have shown that LZ-C is involved in the tetramer formation of TH and disruption of LZ-C abolishes the tetramer assemble in mammalian cells [87], and similarly observation has been reported for the enzyme recombinantly expressed in bacteria [22]. Thus, it is noteworthy that TH could exist in different forms other than tetrameric but this work has shown that TH does not seem to exist as dimer upon phosphorylation at Ser19 and/or nuclear localization.

6.3 Subcellular distribution of TH

TH has been considered a cytosolic enzyme until the recent finding by Nakashima et al. showing that THpSer19 was distributed in the nucleus of PC12 cells [71]. However, the mechanism of nuclear localization or its possible physiological relevance was not explained. We investigated the subcellular distribution of endogenous and recombinant TH to show if the nuclear localization is dependent on Ser19 phosphorylation. We were able to reproduce the finding of Nakashima et al, by using a specific antibody against pSer19, as it was observed that the THpSer19 was predominantly distributed in the nucleus of neuroblastoma cells. However, Western blot results were contradicting. Although, THpSer19 was found in the nuclear fraction, the band intensity in cytosolic fraction (per amount of protein) was stronger.

Immunofluorescence (IF) is a technique that preserves protein:protein interactions whereas Western blot is a denaturing method. In addition, it is well established that THpSer19 binds to the proteins of the 14-3-3 family in a phospho-Ser19 specific manner [72]. Thus, we hypothesized that binding to 14-3-3 and maybe other partners, may hinder the access of the antibodies to the phosphorylation site in the cytoplasm when performing our *in situ* immunofluorescence assays. Therefore, we detected THpSer19 by IF in neuroblastoma samples previously treated with a denaturing agent such as 6M GuHCl (Figure 5.13). Although, the THpSer19 showed an intense nuclear signal, the cytoplasmic intensity was increased in the presence of GuHCl.

We also expressed V5-TH constructs (Wt, S19A and S19E) in neuroblastoma cells to investigate if the nuclear localization is Ser19 phosphorylation dependent using three different techniques: IF, Western blot and PLA. Our results indicate that the level of recombinant TH-Wt was higher in the nucleus when compared to V5-TH-S19A and V5-TH-S19E. Moreover, V5-TH-S19E showed variability in the phosphorylation studies, leading us to an understanding that phospho mimic mutant failed to fully reflect the effect of phosphorylation. This conclusion is also supported by the preliminary data from our group, i.e THpS19E does not bind to 14-3-3. The reason could be that the phosphate group (PO_4^{3-}) is chemically distinct from the negatively charged amino acid such as Glu or Asp, because PO_4^{3-} has large hydrated shell and negative charge greater than 1, whereas Asp and Glu have single negatively charged side chain and smaller hydrated shell. It has been suggested by Peralman et al. that a pair of Glu or Asp residues in a vicinity might serve as a better

phosphomimetic mutation than a single Glu or Asp, since this would provide a double negatively charged microenvironment [88].

Although it was not clear if the distribution of TH in the nucleus is phosphorylation dependent, PLA analysis, however, clearly indicated that the TH distributed in the nucleus was most probably phosphorylated at Ser19 (Figure 5.22).

6.4 THpSer19 and 14-3-3 interaction

By using IF, we investigated the co-distribution of endogenous TH and 14-3-3. Confocal images clearly illustrated that both TH and 14-3-3 proteins were distributed in both the cytoplasm and nucleus of neuroblastoma cells (Figure 5.26A) but the signal intensity was weak, which could be due to the interaction of TH and 14-3-3 to their respective binding partner, the epitope of protein that is recognized by antibody is masked. To prove the point we treated the samples with denaturing agent GuHCl which could break the interaction and expose the masked epitopes to be recognized by the respective antibodies. It was clear from the IF images obtained by using confocal microscope, that the signal intensity, especially in the cytoplasm, was much higher after the treatment with GuHCl (Figure 5.26B).

As we found out that both TH and 14-3-3 were distributed in the nucleus, we investigated if these proteins were partners in the nucleus as well. Focusing in the nucleus of neuroblastoma cells, we carried out PLA to detect protein:protein interaction between recombinant TH and 14-3-3, regardless of 14-3-3 isoform. It was clear from the PLA analysis that the 14-3-3 present in the nucleus was interacting with THpSer19 (Figure 5.28). We also investigated the specific interaction of THpSer19 with isoform γ of 14-3-3, an isoform that is very abundant in neurons [89]. Our results show that the complex THpSer19:14-3-3γ was predominantly distributed in the cytoplasm and sparsely distributed in the nucleus of neuroblastoma cells.

The 14-3-3 protein family is said to be involved in nearly all cellular processes [50] ranging from transcription, regulation of cell cycle, intracellular trafficking and targeting, cytoskeletal structure and transcription [40] to apoptosis [51]. Previous studies have clearly indicated that phosphorylation of TH at Ser19 by CaMPK II facilitates binding to 14-3-3 proteins [31, 56, 72]. Gorbani et al. have shown that all 14-3-3 homodimers and their respective 14-3-3ε-heterodimers bind to TH phosphorylated at Ser19 with similar high affinity [90]. Furthermore, Wang et al. showed that 14-3-3ζ interaction with TH but not η isoform of 14-3-3 in MN9D cells [60]. Moreover, they also showed that TH associated with the ζ isoform of

14-3-3 was localized to the mitochondria of MN9D cells. They predicted that this interaction of 14-3-3ζ with TH localized to mitochondria may block TH dephosphorylation. Furthermore, Nakashima et al. reported that the 14-3-3η isoform increases the intercellular stability of TH in PC12 cells [91], whereas Sato et al. reported that14-3-3η interacts with the E3-ubiquitin ligase Parkin, and is regulated by α-synuclein [92], an interaction that might be related to recent findings showing that phosphorylation of Ser19 in the N-terminal portion of TH is a trigger for the degradation of the enzyme by the ubiquitin-proteasome pathway [77]. Moreover, our data illustrating the interaction of THpS19 with 14-3-3γ, along with these earlier findings indicate a complex regulatory relationships between 14-3-3 and TH.

6.5 Concluding remarks

Based on the observation from CN-PAGE and BN-PAGE, we propose that the oligomeric state of TH is similar in nucleus and cytosol of neuroblastoma cells. Moreover, the cellular preparations indicate a more homogeneus oligomeric state of TH in cells than for the purified hTH1, which distributes in various forms ranging from octameric/tetrameric to monomeric.

It is also clear from this work that TH is predominantly a cytosolic protein but also distributed in the nucleus, especially when phosphorylated at Ser19. However, there is no sufficient support for a specific nuclear localization of pSer19 in the nucleus, since the major population appears in the cytosol. So the conclusion by Nakashima et al. that generated so much thinking on a possible transcriptional related role for this form of the enzyme might have been unsubstantiated and preliminary.

From this work it has also been shown that THpSer19 interacts with 14-3-3 proteins in both the nucleus and the cytoplasm of neuroblastoma cells, as substantiated by PLA analysis on the distribution of THpSer19:14-3-3γ.

Lastly, this Master thesis has allowed to develop and characterize a set of constructs for the study of TH phosphorylation as well as to standardize protocols for immunofluorescence and PLA quantification. It has also enabled to better understand the different results obtained with complementary methods, in particular the quantification of the subcellular localization of TH using immunofluorescence or Western blot. These tools and knowledge will be used in the lab's future projects that will help unravel the role of phosphorylation in TH.

6.6 Future perspective

In order to better understand the mechanism of nuclear localization of the THpS19, high-throughput genome editing tool, such as CRISPR/Cas9, could be used to induce specific mutation in TH at Ser19 in a cell line (neuroblastoma cells) to create stable phospho-null and phospho-mimicking mutants that would be expressed at physiological levels instead of overexpression. This tool would enable us to study in a less artificial way if the nuclear localization of TH is dependent on Ser19 phosphorylation. Moreover, super resolution confocal microscope could help determining if the distribution around the nuclear envelope is in fact cytosolic or nuclear THpSer19.

Given that the nuclear localization of TH is not strongly dependent on phosphorylation of ThSer19 it would be interesting to analyse the effect of the other phosphorylation sites, Thr8, Ser31 and Ser40 residues, on the nuclear distribution, and how the combination of phosphorylation sites might play a role. It would be particularly interesting to analyse if the phosphorylation of Thr8 is involved because it is a site which has been studied very little and no clear function has been attributed to it.

To gain further insights into the function of THpSer19, the nuclear interaction of THpSer19 with all the isoforms of 14-3-3 proteins should be studied by over-expression of the constructs in neuroblastoma cells and proximity ligation assays combined with confocal microscopy. The results could be verified by pull-down of the tagged protein in nuclear-enriched cellular fractions and detection of 14-3-3 by Western blot.

Lastly, and based on the increased understanding of 14-3-3 proteins as redox regulators of their partners [93, 94], the interaction of TH and 14-3-3, as well as TH activity, purified proteins should be used. The effect of different redox conditions on the binding affinity should be studied both from the THpSer19:14-3-3 interaction and the TH activity perspective, using surface plasmon resonance and HPLC-activity assays, respectively.

7. REFERENCES

1. Lott, F.E. and P. Hudson, *Some Experiments on the Diastatic Power of Malt.* Journal of the Federated Institutes of Brewing, 1895. **1**(4): p. 403-422.
2. Sumner, J.B., *The isolation and crystallization of the enzyme urease preliminary paper.* Journal of Biological Chemistry, 1926. **69**(2): p. 435-441.
3. Anfinsen, C.B., et al., *THE KINETICS OF FORMATION OF NATIVE RIBONUCLEASE DURING OXIDATION OF THE REDUCED POLYPEPTIDE CHAIN.* Proceedings of the National Academy of Sciences of the United States of America, 1961. **47**(9): p. 1309-1314.
4. Anfinsen, C.B., *Principles that govern the folding of protein chains.* Science, 1973. **181**(4096): p. 223-30.
5. Anfinsen, C.B., *Principles that Govern the Folding of Protein Chains.* Science, 1973. **181**(4096): p. 223-230.
6. Dunaway-Mariano, D., *Enzyme Function Discovery.* Structure, 2008. **16**(11): p. 1599-1600.
7. Porter, C.T., G.J. Bartlett, and J.M. Thornton, *The Catalytic Site Atlas: a resource of catalytic sites and residues identified in enzymes using structural data.* Nucleic Acids Research, 2004. **32**(Database issue): p. D129-D133.
8. Suzuki, H., *"Chapter 7: Active Site Structure".* How Enzymes Work: From Structure to Function. Boca Raton, FL: CRC Press., 2015: p. 117-140.
9. Hunter, T., *Protein kinases and phosphatases: The Yin and Yang of protein phosphorylation and signaling.* Cell, 1995. **80**(2): p. 225-236.
10. Cooper, G., *The Central Role of Enzymes as Biological Catalysts.* . The Cell: A Molecular Approach., 2000. **2nd edition.**(Sunderland (MA): Sinauer Associates).
11. Anthony W. Norman, G.L., *Hormone action and biochemistry.* Hormone. Academic press, INC. Orlando, Florida 32887, 2014: p. 463.
12. Haavik, J. and K. Toska, *Tyrosine hydroxylase and Parkinson's disease.* Molecular Neurobiology. **16**(3): p. 285-309.
13. Kumar, G.K. and N.R. Prabhakar, *POST-TRANSLATIONAL MODIFICATION OF PROTEINS DURING INTERMITTENT HYPOXIA.* Respiratory physiology & neurobiology, 2008. **164**(1-2): p. 272-276.
14. Kleppe, R., et al., *Phosphorylation Dependence and Stoichiometry of the Complex Formed by Tyrosine Hydroxylase and 14-3-3γ.* Molecular & Cellular Proteomics, 2014. **13**(8): p. 2017-2030.
15. Flatmark, T. and R.C. Stevens, *Structural Insight into the Aromatic Amino Acid Hydroxylases and Their Disease-Related Mutant Forms.* Chemical Reviews, 1999. **99**(8): p. 2137-2160.
16. Németh, A.H., *The genetics of primary dystonias and related disorders.* Brain, 2002. **125**(4): p. 695-721.
17. Thöny, B., G. Auerbach, and N. Blau, *Tetrahydrobiopterin biosynthesis, regeneration and functions.* Biochemical Journal, 2000. **347**(Pt 1): p. 1-16.
18. Nagatsu, T., *Tyrosine hydroxylase: human isoforms, structure and regulation in physiology and pathology.* Essays Biochem, 1995. **30**: p. 15-35.
19. Daubner, S.C., T. Le, and S. Wang, *Tyrosine hydroxylase and regulation of dopamine synthesis.* Arch Biochem Biophys, 2011. **508**(1): p. 1-12.
20. Grima, B., et al., *A single human gene encoding multiple tyrosine hydroxylases with different predicted functional characteristics.* Nature, 1987. **326**(6114): p. 707-711.
21. Kumer, S.C. and K.E. Vrana, *Intricate Regulation of Tyrosine Hydroxylase Activity and Gene Expression.* Journal of Neurochemistry, 1996. **67**(2): p. 443-462.
22. Vrana, K.E., et al., *A carboxyl terminal leucine zipper is required for tyrosine hydroxylase tetramer formation.* J Neurochem, 1994. **63**(6): p. 2014-20.

23. Fitzpatrick, P.F., *Tetrahydropterin-Dependent Amino Acid Hydroxylases.* Annual Review of Biochemistry, 1999. **68**(1): p. 355-381.
24. Martinez, A., et al., *Conformation and interaction of phenylalanine with the divalent cation at the active site of human recombinant tyrosine hydroxylase as determined by proton NMR.* Biochemistry, 1993. **32**(25): p. 6381-6390.
25. Ramsey, A.J., et al., *Identification of iron ligands in tyrosine hydroxylase by mutagenesis of conserved histidinyl residues.* Protein Science : A Publication of the Protein Society, 1995. **4**(10): p. 2082-2086.
26. Dunkley, P.R., et al., *Tyrosine hydroxylase phosphorylation: regulation and consequences.* Journal of Neurochemistry, 2004. **91**(5): p. 1025-1043.
27. Roskoski, R. and L.M. Roskoski, *Activation of Tyrosine Hydroxylase in PC12 Cells by the Cyclic GMP and Cyclic AMP Second Messenger Systems.* Journal of Neurochemistry, 1987. **48**(1): p. 236-242.
28. Daubner, S.C., et al., *Site-directed mutagenesis of serine 40 of rat tyrosine hydroxylase. Effects of dopamine and cAMP-dependent phosphorylation on enzyme activity.* J Biol Chem, 1992. **267**(18): p. 12639-46.
29. Haycock, J.W., et al., *ERK1 and ERK2, two microtubule-associated protein 2 kinases, mediate the phosphorylation of tyrosine hydroxylase at serine-31 in situ.* Proceedings of the National Academy of Sciences of the United States of America, 1992. **89**(6): p. 2365-2369.
30. Andersson, K.K., et al., *Purification and characterization of the blue-green rat phaeochromocytoma (PC12) tyrosine hydroxylase with a dopamine-Fe(III) complex. Reversal of the endogenous feedback inhibition by phosphorylation of serine-40.* Biochemical Journal, 1992. **284**(Pt 3): p. 687-695.
31. Ichimura, T., et al., *Molecular cloning of cDNA coding for brain-specific 14-3-3 protein, a protein kinase-dependent activator of tyrosine and tryptophan hydroxylases.* Proceedings of the National Academy of Sciences of the United States of America, 1988. **85**(19): p. 7084-7088.
32. Salvatore, M.F. and B.S. Pruett, *Dichotomy of Tyrosine Hydroxylase and Dopamine Regulation between Somatodendritic and Terminal Field Areas of Nigrostriatal and Mesoaccumbens Pathways.* PLoS ONE, 2012. **7**(1): p. e29867.
33. Campbell, D.G., D.G. Hardie, and P.R. Vulliet, *Identification of four phosphorylation sites in the N-terminal region of tyrosine hydroxylase.* J Biol Chem, 1986. **261**(23): p. 10489-92.
34. Lehmann, I.T., et al., *Differential regulation of the human tyrosine hydroxylase isoforms via hierarchical phosphorylation.* J Biol Chem, 2006. **281**(26): p. 17644-51.
35. Sutherland, C., et al., *Phosphorylation and activation of human tyrosine hydroxylase in vitro by mitogen-activated protein (MAP) kinase and MAP-kinase-activated kinases 1 and 2.* Eur J Biochem, 1993. **217**(2): p. 715-22.
36. Toska, K., et al., *Regulation of tyrosine hydroxylase by stress-activated protein kinases.* Journal of Neurochemistry, 2002. **83**(4): p. 775-783.
37. Obeso, J.A., et al., *Missing pieces in the Parkinson's disease puzzle.* Nat Med, 2010. **16**(6): p. 653-661.
38. Wijemanne, S. and J. Jankovic, *Dopa-responsive dystonia[mdash]clinical and genetic heterogeneity.* Nat Rev Neurol, 2015. **11**(7): p. 414-424.
39. Willemsen, M.A., et al., *Tyrosine hydroxylase deficiency: a treatable disorder of brain catecholamine biosynthesis.* Brain, 2010. **133**(6): p. 1810-1822.
40. Aitken, A., *14-3-3 proteins: A historic overview.* Seminars in Cancer Biology, 2006. **16**(3): p. 162-172.
41. Cockrell, L.M., et al., *14-3-3 Proteins*, in *Wiley Encyclopedia of Chemical Biology*. 2007, John Wiley & Sons, Inc.
42. Toker, A., et al., *Multiple isoforms of a protein kinase C inhibitor (KCIP-1/14-3-3) from sheep brain.* European Journal of Biochemistry, 1992. **206**(2): p. 453-461.

43. Bridges, D. and G.B.G. Moorhead, *14-3-3 Proteins: A Number of Functions for a Numbered Protein.* Science Signaling, 2005. **2005**(296): p. re10-re10.
44. Liu, D., et al., *Crystal structure of the zeta isoform of the 14-3-3 protein.* Nature, 1995. **376**(6536): p. 191-194.
45. Xiao, B., et al., *Structure of a 14-3-3 protein and implications for coordination of multiple signalling pathways.* Nature, 1995. **376**(6536): p. 188-191.
46. Fu, H., R.R. Subramanian, and S.C. Masters, *14-3-3 Proteins: Structure, Function, and Regulation.* Annual Review of Pharmacology and Toxicology, 2000. **40**(1): p. 617-647.
47. Aitken, A., et al., *14-3-3 and Are the Phosphorylated Forms of Raf-activating 14-3-3 and : IN VIVO STOICHIOMETRIC PHOSPHORYLATION IN BRAIN AT A Ser-Pro-Glu-Lys MOTIF.* Journal of Biological Chemistry, 1995. **270**(11): p. 5706-5709.
48. Pozuelo Rubio, M., et al., *14-3-3-affinity purification of over 200 human phosphoproteins reveals new links to regulation of cellular metabolism, proliferation and trafficking.* Biochemical Journal, 2004. **379**(Pt 2): p. 395-408.
49. Kjarland, E., T.J. Keen, and R. Kleppe, *Does Isoform Diversity Explain Functional Differences in the 14-3-3Protein Family?* Current Pharmaceutical Biotechnology, 2006. **7**(3): p. 217-223.
50. Paul, G. and H. van Heusden, *14-3-3 Proteins: Regulators of numerous eukaryotic proteins.* IUBMB Life, 2005. **57**(9): p. 623-629.
51. Rosenquist, M., et al., *Evolution of the 14-3-3 protein family: does the large number of isoforms in multicellular organisms reflect functional specificity?* J Mol Evol, 2000. **51**(5): p. 446-58.
52. Zannis-Hadjopoulos, M., W. Yahyaoui, and M. Callejo, *14-3-3 Cruciform-binding proteins as regulators of eukaryotic DNA replication.* Trends in Biochemical Sciences. **33**(1): p. 44-50.
53. Yamauchi, T., H. Nakata, and H. Fujisawa, *A new activator protein that activates tryptophan 5-monooxygenase and tyrosine 3-monooxygenase in the presence of Ca2+-, calmodulin-dependent protein kinase. Purification and characterization.* Journal of Biological Chemistry, 1981. **256**(11): p. 5404-5409.
54. Atkinson, J., et al., *Phosphorylation of Purified Rat Striatal Tyrosine Hydroxylase by Ca2+/Calmodulin-Dependent Protein Kinase II: Effect of an Activator Protein.* Journal of Neurochemistry, 1987. **49**(4): p. 1241-1249.
55. Tanji, M., et al., *Activation of Protein Kinase C by Purified Bovine Brain 14-3-3: Comparison with Tyrosine Hydroxylase Activation.* Journal of Neurochemistry, 1994. **63**(5): p. 1908-1916.
56. Itagaki, C., et al., *Stimulus-Coupled Interaction of Tyrosine Hydroxylase with 14-3-3 Proteins.* Biochemistry, 1999. **38**(47): p. 15673-15680.
57. Kleppe, R., K. Toska, and J. Haavik, *Interaction of phosphorylated tyrosine hydroxylase with 14-3-3 proteins: evidence for a phosphoserine 40-dependent association.* Journal of Neurochemistry, 2001. **77**(4): p. 1097-1107.
58. Kleppe, R., et al., *The 14-3-3 proteins in regulation of cellular metabolism.* Seminars in Cell & Developmental Biology, 2011. **22**(7): p. 713-719.
59. Schindler, C.K., M. Heverin, and D.C. Henshall, *Isoform- and subcellular fraction-specific differences in hippocampal 14-3-3 levels following experimentally evoked seizures and in human temporal lobe epilepsy.* Journal of Neurochemistry, 2006. **99**(2): p. 561-569.
60. Wang, J., et al., *14-3-3ζ Contributes to Tyrosine Hydroxylase Activity in MN9D Cells: LOCALIZATION OF DOPAMINE REGULATORY PROTEINS TO MITOCHONDRIA.* Journal of Biological Chemistry, 2009. **284**(21): p. 14011-14019.
61. Ding, H., et al., *14-3-3 inhibition promotes dopaminergic neuron loss and 14-3-3ϑ overexpression promotes recovery in the MPTP mouse model of Parkinson's disease.* Neuroscience, 2015. **307**: p. 73-82.
62. Sanger, F., S. Nicklen, and A.R. Coulson, *DNA sequencing with chain-terminating inhibitors.* Proceedings of the National Academy of Sciences of the United States of America, 1977. **74**(12): p. 5463-5467.

63. Wittig, I. and H. Schägger, *Advantages and limitations of clear-native PAGE.* PROTEOMICS, 2005. **5**(17): p. 4338-4346.
64. Wittig, I., H.-P. Braun, and H. Schagger, *Blue native PAGE.* Nat. Protocols, 2006. **1**(1): p. 418-428.
65. Schägger, H. and G. von Jagow, *Blue native electrophoresis for isolation of membrane protein complexes in enzymatically active form.* Analytical Biochemistry, 1991. **199**(2): p. 223-231.
66. Schagger, H., W.A. Cramer, and G. Vonjagow, *Analysis of Molecular Masses and Oligomeric States of Protein Complexes by Blue Native Electrophoresis and Isolation of Membrane Protein Complexes by Two-Dimensional Native Electrophoresis.* Analytical Biochemistry, 1994. **217**(2): p. 220-230.
67. Fredriksson, S., et al., *Protein detection using proximity-dependent DNA ligation assays.* Nat Biotech, 2002. **20**(5): p. 473-477.
68. *"Principle of in situ PLA". http://www.antibodies-online.com/resources/17/1258/Matched+antibody+pairs+for+various+purposes/.* April 2016.
69. K Reynaud[1,] D.N., R Cortvrindt[1], R Kurzawa[2], J Smitz[1], *Confocal microscopy: principles and applications to the field of reproductive biology.* Folia Histochemica et Cytobiologica, 2001. **39**(2): p. 75-85.
70. S.W. Paddock, T.J.F.a.M.W.D., *"Basic concept". http://www.microscopyu.com/articles/confocalintrobasics.html,.* April 2016.
71. Nakashima, A., et al., *Phosphorylation of the N-terminal portion of tyrosine hydroxylase triggers proteasomal digestion of the enzyme.* Biochemical and Biophysical Research Communications, 2011. **407**(2): p. 343-347.
72. Ichimura, T., et al., *Brain 14-3-3 protein is an activator protein that activates tryptophan 5-monooxygenase and tyrosine 3-monooxygenase in the presence of Ca2+,calmodulin-dependent protein kinase II.* FEBS Lett, 1987. **219**(1): p. 79-82.
73. Obsilova, V., et al., *The 14-3-3 protein affects the conformation of the regulatory domain of human tyrosine hydroxylase.* Biochemistry, 2008. **47**(6): p. 1768-77.
74. Hunter, T., *Why nature chose phosphate to modify proteins.* Philosophical Transactions of the Royal Society of London B: Biological Sciences, 2012. **367**(1602): p. 2513-2516.
75. Canagarajah, B.J., et al., *Activation Mechanism of the MAP Kinase ERK2 by Dual Phosphorylation.* Cell, 1997. **90**(5): p. 859-869.
76. Miranda, F.F., et al., *Phosphorylation and mutations of Ser(16) in human phenylalanine hydroxylase. Kinetic and structural effects.* J Biol Chem, 2002. **277**(43): p. 40937-43.
77. Nakashima, A., et al., *Inhibition of deubiquitinating activity of USP14 decreases tyrosine hydroxylase phosphorylated at Ser19 in PC12D cells.* Biochem Biophys Res Commun, 2016. **472**(4): p. 598-602.
78. Albert, K.A., et al., *Calcium/phospholipid-dependent protein kinase (protein kinase C) phosphorylates and activates tyrosine hydroxylase.* Proceedings of the National Academy of Sciences of the United States of America, 1984. **81**(24): p. 7713-7717.
79. Vulliet, P.R., J.R. Woodgett, and P. Cohen, *Phosphorylation of tyrosine hydroxylase by calmodulin-dependent multiprotein kinase.* J Biol Chem, 1984. **259**(22): p. 13680-3.
80. Szmigielski, A., A. Guidotti, and E. Costa, *Endogenous protein kinase inhibitors. Purification, characterization, and distribution in different tissues.* J Biol Chem, 1977. **252**(11): p. 3848-53.
81. Hurley, J.H., et al., *Regulation of an enzyme by phosphorylation at the active site.* Science, 1990. **249**(4972): p. 1012-6.
82. Kaufman, S., *Tyrosine Hydroxylase*, in *Advances in Enzymology and Related Areas of Molecular Biology*. 2006, John Wiley & Sons, Inc. p. 103-220.
83. Haycock, J.W. and D.A. Haycock, *Tyrosine hydroxylase in rat brain dopaminergic nerve terminals. Multiple-site phosphorylation in vivo and in synaptosomes.* J Biol Chem, 1991. **266**(9): p. 5650-7.

84. Ficner, R., et al., *Three-dimensional structure of the bifunctional protein PCD/DCoH, a cytoplasmic enzyme interacting with transcription factor HNF1.* Embo j, 1995. **14**(9): p. 2034-42.
85. Goodwill, K.E., et al., *Crystal structure of tyrosine hydroxylase at 2.3 A and its implications for inherited neurodegenerative diseases.* Nat Struct Biol, 1997. **4**(7): p. 578-85.
86. Liu, X. and K.E. Vrana, *Leucine zippers and coiled-coils in the aromatic amino acid hydroxylases.* Neurochem Int, 1991. **18**(1): p. 27-31.
87. He, X., et al., *Relationship between enzymatic activity and oligomerization state of tyrosine hydroxylase.* Journal of Biomedical Science, 1996. **3**(5): p. 332-337.
88. Pearlman, S.M., Z. Serber, and J.E. Ferrell, Jr., *A mechanism for the evolution of phosphorylation sites.* Cell, 2011. **147**(4): p. 934-46.
89. Martin, H., et al., *Subcellular localisation of 14-3-3 isoforms in rat brain using specific antibodies.* J Neurochem, 1994. **63**(6): p. 2259-65.
90. Ghorbani, S., et al., *Regulation of tyrosine hydroxylase is preserved across different homo- and heterodimeric 14-3-3 proteins.* Amino Acids, 2016. **48**(5): p. 1221-1229.
91. Nakashima, A., et al., *RNAi of 14-3-3eta protein increases intracellular stability of tyrosine hydroxylase.* Biochem Biophys Res Commun, 2007. **363**(3): p. 817-21.
92. Sato, S., et al., *14-3-3eta is a novel regulator of parkin ubiquitin ligase.* Embo j, 2006. **25**(1): p. 211-21.
93. Kim, J.S., T.Y. Huang, and G.M. Bokoch, *Reactive oxygen species regulate a slingshot-cofilin activation pathway.* Mol Biol Cell, 2009. **20**(11): p. 2650-60.
94. Jeon, Y.H., et al., *Identification of a redox-modulatory interaction between selenoprotein W and 14-3-3 protein.* Biochim Biophys Acta, 2016. **1863**(1): p. 10-8.